UNIVERSITÀ DEGLI STUDI DI PADOVA

DIPARTIMENTO DI BIOLOGIA

Corso di Laurea magistrale in Molecular Biology

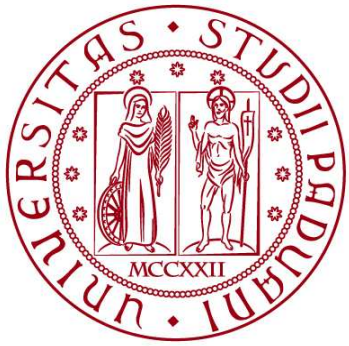

TESI DI LAUREA

Assessing molecular and cellular consequences of the LRRK2:14-3-3 complex

Relatore: Prof.ssa Elisa Greggio
Dipartimento di Biologia

Correlatore: Prof. Jean-Marc Taymans
Lille Neuroscience & Cognition – Faculté de Medicine – Université de Lille

Laureando: Alessio Burin

ANNO ACCADEMICO 2022/2023

Acknowledgements

After a long and challenging journey, I arrive at the end of my university studies. This chapter of my life has closed in a most wonderful way, with the opportunity of taking part in the scientific community with the work of my own hands. For this, I must first and foremost thank my professors, prof. Elisa Greggio from the University of Padova and prof. Jean-Marc Taymans from the University of Lille, where my internship has taken place. Under their watchful and careful guidance, I was able to create the work I am proud to present to you.

A special thanks must be made to Antonio J. Lara Ordóñez, who taught me, helped me, advised me in every part of life inside the lab. No matter the circumstances, he always helped me correcting my mistakes, giving me tips, advising on how to face an unexpected result.

I am also grateful to the team forming the lab, including Sergio Hernandez, Adriana Figueroa Garcia, Chloé Annicotte, Baptiste Damary, Georgia Louskou, Mathilde Coevoet, Catherine Baud, Staelle Corvo-Chamaillard, Benedicte Vanteghem. They showed me how the laboratory can only work at its best when everyone is doing their part, and how you can count on your colleagues to help in times of need. Not only that, but they also showed me how one can build a great relationship with its colleagues and create an environment of conviviality.

Of course, none of this would be possible without my parents, my brother, my family, my girlfriend and all my loved ones, who have never stopped believing in me and pushing me forward to where I stand now. I owe to them everything.

Table of contents

1. List of abbreviations

Parkinson's disease: PD

Leucine Rich Repeat Kinase 2: LRRK2

Neurodegenerative diseases: NDD

Central Nervous System: CNS

Peripheral Nervous System: PNS

Alzheimer's disease: AD

Substantia Nigra pars compacta: *SNpc*

Genome-Wide Association Studies: GWAS

PTEN-induced kinase 1: PINK1

Blood-brain barrier: BBB

Ras of Complex: ROC

C-terminal of ROC: COR

Tyrosine kinase-like family: TKL

Armadillo Repeat Motifs: ARM

Ankyrin: ANK

Leucine-Rich Repeat: LRR

Kinase domain: KIN

Knockout: KO

Protein Phosphatase 1: PP1

Protein Phosphatase 2: PP2

Lysogeny broth: LB

Rotations per minute: RPM

Human Embryonic Kidney: HEK

Dulbecco's Modified Eagle Medium: DMEM

Dulbecco's Phosphate Buffered Saline: PBS

Dimethyl sulfoxide: DMSO

Relative centrifugal field: rcf

Bicinchoninic acid assay: BCA

Bovine serum albumin: BSA

Phosphorylated serine 935: pS935

Paraformaldehyde: PFA

Immunocytochemistry: ICC

Horse Radish Peroxidase: HRP

Immunoprecipitate: IP

Biotin identification: BioID

Multivesicular body: MVB

Extracellular vesicle: EV

Deoxyribonucleic acid: DNA

Ribonucleic acid: RNA

Reactive Oxygen Species: ROS

Rapid Eye Movement: REM

2. Abstract

Parkinson's disease (PD) is the second most common progressive neurodegenerative disorder. The *Leucine Rich Repeat Kinase 2* (*LRRK2*) gene is mutated in some familial PD cases and in idiopathic PD. Most LRRK2-PD mutations result in a protein with increased kinase activity. LRRK2 kinase inhibitors revert disease-associated phenotypes in cells, but they can cause abnormalities in LRRK2-expressing tissues. When interacting with 14-3-3, LRRK2 is maintained in a less active cytosolic form. This LRRK2:14-3-3 complex requires the phosphorylation of serine 910 and serine 935 within LRRK2, which is decreased in PD-associated mutants. Therefore, our working hypothesis is that preserving the LRRK2:14-3-3 complex is beneficial against PD. In this work, biomolecular and cellular phenotypes of the LRRK2:14-3-3 complex have been determined, with the aim of assessing in the future the activity of compounds able to increase the affinity of the complex. Phenotypes of phospho-dead and phospho-mimicking LRRK2 mutants have also been studied, to develop reliable controls of the interaction. Our results show that a 6xS>A phospho-dead mutant is a valid negative control, but do not validate a phospho-mimicking 6xS>D LRRK2 as a positive control. These results could help the development of effective new treatments for PD, by modulating LRRK2 activity via its interactors.

3. Introduction

The term Parkinson's disease (PD) refers to a neurodegenerative disorder that affects millions of people worldwide, with an estimated 10 million patients currently living with the condition. In fact, it is the second most common progressive neurodegenerative disorder in the world, after Alzheimer's disease, and reports show its incidence is growing, making PD the fastest growing neurological condition worldwide. This is expected to increase pressure on the healthcare system, as patients need continuous social and medical support. Furthermore, it is a complex disease, with a wide range of symptoms. This complicates the diagnosis and proper care that must be tailored to each individual patient.

For these reasons, PD has been an important topic for medical, neurological, and biological research. Even if a cure is currently not available, research on the causes, mechanisms and symptoms of the condition has helped to gain much deeper insight into the functioning of the disease. Naturally, the final objective remains to find better ways to care for patients, mitigate symptoms and ultimately find a cure.

The work of the present master thesis is focused on the molecular and cellular mechanisms behind PD, focusing on the role of Leucine-Rich Repeat Kinase 2 (LRRK2) in the context of the disease. This protein is involved in a wide variety of important cellular processes altered in PD, and was shown to be altered in PD patients, making it an interesting therapeutic target.

3.1. Neurodegenerative diseases

Neurodegenerative diseases (NDDs) are a heterogeneous group of conditions that affect either the Central Nervous System (CNS) or the Peripheral Nervous System (PNS), causing a progressive loss of neurons. Since neurons are terminally differentiated cells and cannot renew themselves, any damage to these systems has serious and often permanent effects on the patient's well-being. Symptoms vary significantly between diseases, depending on the type of neurons lost. Examples of NDDs are Alzheimer's disease (AD), amyotrophic lateral sclerosis, Lewy body dementia, prion disease and PD. Neurodegenerative diseases have some key common factors, named hallmarks of neurodegeneration (Wilson III *et al.*, 2022) (*table 1*).

Table 1 - Hallmarks of neurodegenerative disorders	
Protein aggregation	Protein aggregates are found in brain regions that correlate with clinical symptoms.
Aberrant proteostasis	Altered ubiquitin-proteasome system and autophagy lysosomal pathway lead to accumulation of waste in the cell.
Cytoskeletal abnormalities	Axonal dysfunction contributes to disease progression in many NDDs.
Inflammation	The postmortem brains of patients all show signs of neuroinflammation, which is a source of damage for cells and triggers the immune response.
DNA and RNA defects	Deoxyribonucleic acid (DNA) and ribonucleic acid (RNA) defects can derive from other hallmarks, like inflammation and altered energy homeostasis. Damage to nucleic acids affects gene expression and protein levels, leading to pathological symptoms. DNA damage also correlates with age.
Synaptic network defects	Defects in synapses are found in the specific brain regions connected to clinical symptoms.
Altered energy homeostasis	Neurons demand a high amount of energy. Mitochondrial dysfunction, which can increase ROS production in the cell, is involved in several NDDs.
Neuronal cell death	Hallmark defining all NDDs. Mechanisms vary, with apoptosis, ferroptosis, phagoptosis and necrosis among the documented ones.

Protein aggregation is a prominent pathological phenotype for most NDDs, so much so that these diseases are classified on the base of the aggregating protein. Examples of this are Tau, the aggregating protein in tauopathies, like Alzheimer's disease, and α-synuclein for synucleinopathies.

The highly specialized cell morphology and internal organization of neurons, necessary for their function, is particularly vulnerable to the physiological changes associated with neurodegeneration. Their postmitotic nature causes them to accumulate both age-dependent and environmentally derived (e.g., inflammation) DNA-damage. Proteins can misfold or get damaged by environmental stress and even genes can mutate. This then causes them to accumulate due to the altered proteostasis. Neuron function is dependent on the highly ordered internal cytoskeleton to deliver key components for communication, like neurotransmitters, to their designated cellular localization. This internal order is then lost, causing non-functional synapses. In the end, neurons die, resulting in significant brain volume loss.

3.2. Parkinson's disease

3.2.1. Clinical Symptoms

Most PD cases present motor symptoms, which have been recognised as an important part of the disease since its first description in the 19th century (Kalia, Lang, 2015). These symptoms are comprised of:

1. Bradykinesia, the most important primary motor symptom. It consists in a general movement slowdown and problems with fine motor control.
2. Rigidity, which locks muscles to a state of basal stiffness and reduces the range of movement.
3. Tremor, a rhythmic muscle contraction that affects limb extremities.
4. Postural instability, a symptom that develops in late stages of the disease, and the main cause of PD patients falls.

Motor symptoms are, however, highly variable among patients, both in their prominence and in their development over time. PD also presents non-motor symptoms, which include:

1. Sleep disturbances, like Rapid Eye Movement (REM) behaviour abnormalities
2. Impaired olfaction
3. Cognitive impairment, which often consists in slower thinking and information processing

4. Autonomic dysfunction, which includes gastrointestinal issues such as constipation and orthostatic hypotension

Some of the non-motor symptoms arise much earlier while others develop later in the disease (*figure 1*). Notably, late-stage PD cases show a high incidence of dementia as well, with the symptom being present in 83% of patients who have had the disease for more than 20 years (Kalia, Lang, 2015).

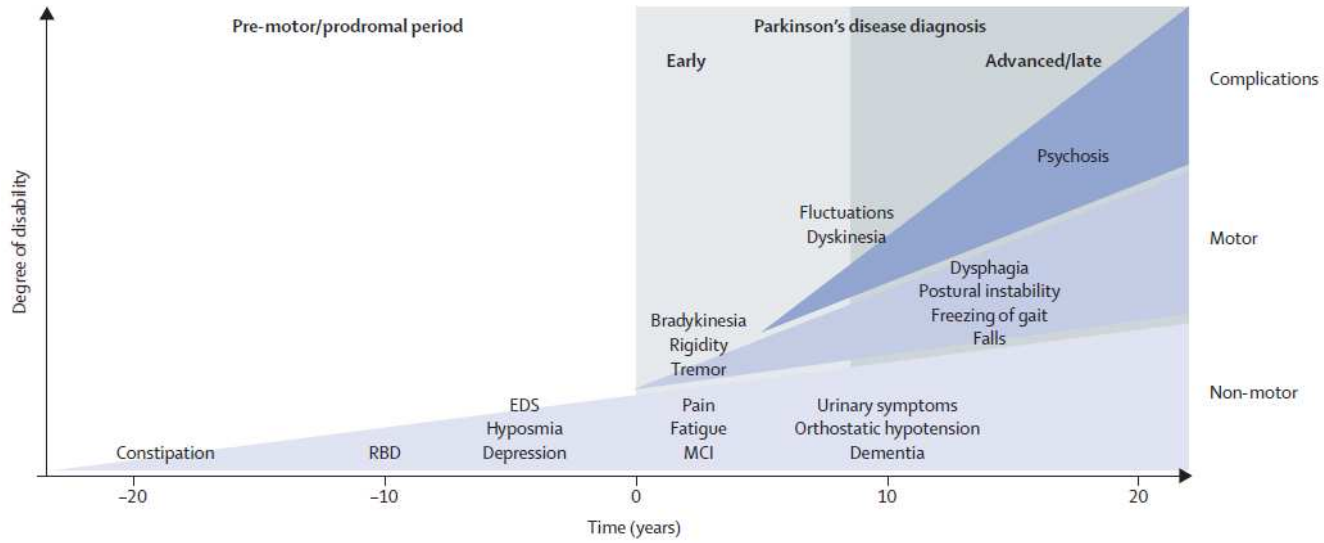

Figure 1 - Clinical symptoms and the time course of Parkinson's disease progression (Kalia et al, 2015).
Parkinson's disease starts at the diagnosis of motor symptoms, represented as 0 years. Many non-motor symptoms can present themselves before diagnosis, in the so-called prodromal period.

3.2.2. Main neuropathological features of Parkinson's disease

Neuronal cell death

The crucial pathological feature of Parkinson's disease is the neuronal cell death of dopaminergic neurons in the *substantia nigra pars compacta* (*SNpc*). This is part of the basal ganglia, which play an important role in the regulation of voluntary movement. The dopamine deficiency that results from the death of dopaminergic neurons is the prime cause of the motor symptoms characterizing PD, but these are not the only neurons affected. Neurons die also in other regions, including the amygdala, the hypothalamus, the locus coeruleus, the nucleus basalis of Meynert (Kalia, Lang, 2015), which could in part explain PD non-motor symptoms.

Lewy Body Formation

Parkinson's disease falls under the NDDs family of α-synucleinopathies, where the aggregate-forming protein is α-synuclein. This is a small (14 kDa) soluble protein found primarily in the CNS. The protein was shown to be able to interact with neurotransmitter-containing-vesicles and several studies show a role for α-synuclein in neurotransmitter release, but its function is still debated and there is no consensus on whether it promotes or inhibits dopamine release (Bendor *et al.*,2013). Crucially, α-synuclein can misfold, causing the formation of aggregates that accumulate in macromolecular structures called Lewy bodies (Srinivasan *et al.*, 2021). A fundamental property of Lewy Bodies in the context of PD is that they

tend to preferentially appear in neurons connected to other neurons that present Lewy bodies. This property is thought to be the result of the uptake of misfolded α-synuclein proteins, which then become the seed for new Lewy bodies (Luk, Lee, 2014). Researchers have proposed that the spreading of these structures occurs in a stereotyped manner, in what is called the Braak Staging of Parkinson's Disease. This model sees the start of Lewy Bodies formation in the PNS, which then arrives at the CNS possibly via the vagus nerve. This model is interesting because the various stages seem to fit the clinical course of the disease: the first stages affect neurons implicated in the premotor symptoms, stage 3 coincides with the development of *SNpc* dopamine deficiency. All of this has led many scientists to hypothesize that one or more steps in Lewy body formation is toxic, but it is not clear whether Lewy bodies themselves are toxic in the context of PD.

3.2.3. Parkinson's disease aetiology

In our current understanding of PD, the disease is multifactorial, with an interplay of genetics, the aging process, and environmental factors at its origin. Cases are divided into either monogenic PD, where a mutation in a single gene causes the disease, or idiopathic PD, where there is no clear cause for the disease, but risk factors have been identified.

Idiopathic PD

Several risk factors, both environmental and genetic, have been found through Genome-Wide Association Studies (GWAS). These studies identified polymorphisms at certain gene *loci* that increase the risk of PD; the list of genes includes, but is not limited to, some of those responsible for monogenic versions of PD.

Age is by far the most important risk factor for PD, with a median age at onset of 60 years (Jankovic, Tan, 2020). Lifestyle factors play an important aspect as well, like pesticide exposure, which increases risk, and caffeine consumption, which is reported to reduce risk (Kalia, Lang, 2015).

Familial PD

Familial PD corresponds to only around 10% of the total cases of PD. These cases are identified by the presence of the pathology across multiple generations in affected families. In the absence of environmental risk factors to which family members may have been exposed, genetic linkage analysis can provide important insight in the pathology of PD in the form of genetic modification in specific genes.

3.2.4. Genetics of Parkinson's disease

Familial Parkinson's disease and the genes involved

Genetic *loci* found to be linked with PD are called *loci PARK* and numbered in chronological order of their discovery. The causative genes behind many of these *loci* have been identified, like *SNCA* for *PARK1* and *PARK4*, but some remain to be discovered. Furthermore, the number of *PARK loci* has kept increasing in recent years, so it is safe to say that the whole picture on the genetics of PD has not yet been obtained.

There are both autosomal dominant forms of monogenic PD and autosomal recessive forms (*table 2*). The latter are rarer, and present a distinct set of symptoms, with an earlier age of onset as a main characteristic.

Table 2 – Genes involved in the main monogenic forms of PD	
Gene and PARK locus/i	**Encoded protein**
	Autosomal Dominant
SNCA *PARK1, PARK4*	**α-synuclein** involved in synaptic plasticity and neuronal differentiation
LRRK2 *PARK8*	**LRRK2** complex kinase and GTPase involved in several processes including neurite growth. Most common gene mutated in familial PD
VPS35 *PARK17*	**VPS35** Component of a complex that associates with endosomes
	Autosomal recessive
PARKIN *PARK2*	**PARKIN** Ubiquitously expressed protein structurally and functionally like ubiquitin ligases that targets cytoplasmic protein for degradation
PINK1 *PARK6*	**PTEN-induced kinase (PINK1)** Serine-threonine kinase localized to the mitochondria
DJ-1 *PARK7*	**Protein deglycase DJ-1** Function of this protein is still unknown, but it has been shown to reallocate to mitochondria in the presence of oxidative stress

There are some key differences in disease course associated to recessive and dominant familial PD patients, the most important of which is the age of onset (Kalia, Lang, 2015). Dominant cases tend to have an age of onset closer to the one

seeing in idiopathic PD (60-70s years old), while recessive cases typically start to show symptoms much earlier in life. As said before, sporadic PD correlates with a variety of genes, which often include, but are not limited to, genes for familial PD.

MAPT

This gene encodes for the Tau protein, a fundamental protein in the context of many different *NDDs*. It is a small protein present in the cytosol that stabilizes microtubules; as such, it is of great relevance for the proper functioning of neurons and for the regulation of axonal transport. Similarly to α-synuclein, Tau protein is an intrinsically disordered protein, but in NDDs it becomes insoluble and assembles. The main NDD associated with Tau protein AD, but it was discovered that Tau, especially when phosphorylated, is also present in the Lewy bodies and that typical Tau pathology, with tangles formation, is observed in 50% of PD patients (Zhang *et al.*, 2018). The interaction between Tau and α-synuclein is thought to significantly affect neuron survival rate (Zhang *et al.*, 2018).

GBA1

The *GBA1* gene encodes the β-glucocerebrosidase enzyme, which is a lysosomial hydrolase responsible for the degradation of glucocerebroside into ceramide and glucose (Gan-or *et al.*, 2018). Glucocerebroside itself is a sphingolipid, component of membranes in cells. Homozygous mutations in *GBA1* are the cause of Gaucher's disease, which is the most common lysosomal storage disease. However, heterozygous mutations in the gene can predispose for PD. In fact, the connection between *GBA1* mutations and PD has been made first through clinical observations, where a strong association was observed (Gan-Or *et al.*, 2018). Later on, GWAS analysis confirmed polymorphism at the *GBA1 locus* to be the most important risk factor for PD (Kalia, Lang, 2015). One of the proposed explanations behind this is the fact that glucocerebroside may lead to α-synuclein accumulation, and α-synuclein can then also lead to decreased activity of the GBA1 enzyme (Gan-Or *et al.*, 2018).

3.2.5. Treatment of Parkinson's disease

Currently, there is no available cure for PD. The treatments currently available can only manage its symptoms, while leaving the neurodegenerative process underlying them unaffected. Treatment of motor symptoms is achieved by managing the decrease in dopamine concentration in the cerebrum (Kalia, Lang, 2015). Systemic administration of dopamine is not a viable option, as the neurotransmitter is not able to pass the blood-brain barrier (BBB). Instead, treatment consists of *levodopa*, an intermediate in the biosynthetic pathway of dopamine, which can pass the BBB and be converted into dopamine.

Ultimately, current symptomatic treatments are insufficient to battle the condition, and in recent decades research has been focusing on studying physiological pathways altered in the disease. This can lead to the identification of key proteins that regulate these pathways and that can be assessed as putative therapeutic targets.

3.3. Leucine-Rich Repeat Kinase 2 (LRRK2)

3.3.1. General knowledge

LRRK2 structure

LRRK2 is a complex protein of 286 kDa and 2527 amino acids, and member of the ROCO protein family. These proteins are characterized by the presence in all members of a GTPase domain called Ras of Complex proteins (ROC), followed by the C-terminal of ROC domain (COR) (*figure 2)*. LRRK2 is therefore a GTPase, but because of the presence of a kinase (KIN) domain, it is also a member of the Tyrosine kinase-like family (TKL), Aside from the ROC, COR and KIN domains, the LRRK2 protein is comprised of other domains. The full extension of the role of each domain is not clear, although similar domains are also found in other proteins, where they were documented to mediate protein-protein interactions. This points to LRRK2's activity being subjected to a fine regulation. It is also true that LRRK2 folds into a complex 3D structure, where the catalytic domains are close to the other domains (*figure 3*), so interaction between protein domains is thought to be important for catalytic activity. Intriguingly, some regions mostly concerning the linkers between different domains, have yet to be determined (*figure 3*). In particular, the LRR domain contains a disordered region with an internal hinge helix (*figure 3*), which is thought to mediate the ability of the ARM domain to freely rotate (Myasnikov *et al*., 2021). LRRK2 is also capable of creating homodimers, which are reported to regulate LRRK2 kinase activity (Soliman *et al.*, 2020).

Table 3 – LRRK2 domains (from N-terminal to C-terminal)

Domain	Function
Armadillo Repeat Motifs (ARM)	Involved in hetero protein-protein interactions, and the activation of the KIN domain by interacting with RAB proteins
Ankyrin Repeat Domain (ANK)	Involved in both hetero protein-protein interaction and homodimer formation
Leucine-Rich Repeat (LRR)	Involved in hetero protein-protein interaction, possible hub for enzymatic-regulating amino acid modifications
Ras-like GTPase (ROC)	GTPase and GTP-binding activity
C-terminal of ROC (COR)	Domain associated with ROC domain in all ROCO proteins. Important in modulating dimerization
Kinase domain (KIN)	Responsible for both autophosphorylation and hetero phosphorylation of LRRK2 targets.
WD40	Domain involved in protein-protein interaction and mediates kinase activity

Figure 2 - LRRK2 domains

LRRK2 domains are represented, starting on the left with the N-terminal ARM domain and ending on the right with the WD40 domain at the protein's C-terminus. The LRR domain includes a disordered portion, with a hinge helix important for relative movements of the ARM domain.

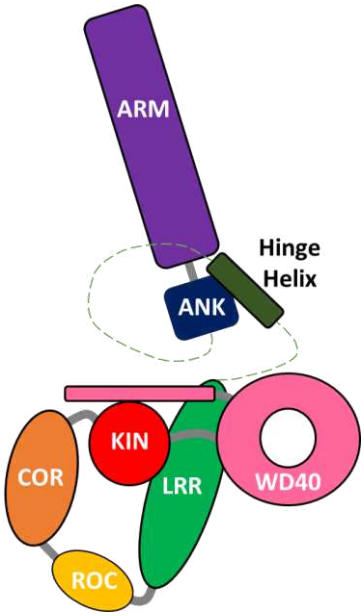

Figure 3 – Cartoon of LRRK2 3D structure

LRRK2 3D structure is presented, showing the disordered region between the ANK and LRR domains, including its hinge helix. The WD40 domain presents a helix that constitutes the C-terminal tail of the protein and is located in close proximity of the KIN domain. This representation illustrates how the domains dedicated to protein-protein interactions are closely interacting the catalytic ones.

LRRK2 physiological subcellular localization

LRRK2 can present itself in different forms and subcellular localizations throughout the cell, which were observed mainly via overexpression of the protein. The most common form of LRRK2 is the monomeric cytosolic version (Berger *et al.*, 2010), bound to the 14-3-3 protein. Crucially, disruption of this interaction is reported to cause the accumulation of LRRK2 in discrete compartments, indicating that 14-3-3 is necessary to stabilize the monomeric cytosolic form of LRRK2 (Nichols *et al.*, 2010). A smaller, but important, fraction of LRRK2 proteins is found bound to membranes in the form of homodimers (Soliman *et al.*, 2010). Crucially, any recruitment of LRRK2 from the cytosol to the cell membrane requires the interaction with proteins from RAB GTPases family. These proteins are involved in vesicular trafficking and the endo-lysosomal pathway and some members of the protein family, such as RAB29, are a known risk factor for PD (Kalia, Lang, 2015). Membrane-recruitment of LRRK2 is important for its function, since LRRK2 is strongly active when in the form of homodimers that form at the membrane level (Usmani *et al.*, 2021). This process extends also to membrane-bound organelles, like vesicles associated with the cell membrane (Usmani *et al.*, 2021).

LRRK2 expression pattern

LRRK2 is expressed at an overall low level throughout the body, with only some specific regions of high expression, these being the lungs, kidneys, and the immune system cells (Miklossy *et al.*, 2006). The overall levels in the brain are modest, but there is high variability between different neural sub-populations. For example, LRRK2 is present in the *SNpc*, but the highest expression is in the putamen, the *SNpc* main output. LRRK2 is also expressed in glial cells, like microglia, astrocytes and oligodendrocytes (Miklossy *et al.*, 2006). These findings suggest a complex physiological role for LRRK2, not limited to the brain.

LRRK2 physiological functions

The physiological role of LRRK2, as well as the scope of its targets and its interactome, have been extensively studied since its discovery, but there are still questions to be answered. Studying knockout (KO) LRRK2 and kinase inhibitors phenotypes can help in determining the cellular processes where the protein is involved, as well as identifying its interactors. Recent research indicates that LRRK2 is implicated in a wide variety of cellular processes, such as membrane trafficking, synaptic transmission in the context of neurons and processes involving the lysosomes, such as autophagy (Wallings *et al.*, 2015).

LRRK2 phosphorylation

One of the most important modifications of LRRK2 to mediate its activity is phosphorylation. Phosphorylated residues can be divided into two main categories: autophosphorylation sites, where the kinase involved is the KIN domain itself, and heterologous phosphorylation sites where different kinases are involved (*figure 4*). Autophosphorylation residues are concentrated in a hotspot around the ROC domain, in the LRR domain and the KIN domain itself. An important autophosphorylation site is the serine S1292, located in the LRR domain, close to ROC. Heterophosphorylation is performed by different kinases, including PKA, CK1α and Ikkβ (Marchand *et al.*, 2020). A major hotspot for heterophosphorylation is present at the N-terminal of the LRR domain, consisting of serines S860, S910, S935, S955, S973 and S976. These heterophosphosites are of significance since they mediate the interaction between LRRK2 and the 14-3-3 protein family. It is important to keep in mind that heterophosphosites are completely independent of the KIN activity. Interestingly inhibition of the kinase domain by type I kinase inhibitors causes a decrease in the phosphorylation of serine 935 (Marchand *et al.*, 2020), and this has been postulated to be due to an inhibitor induced conformational change that recruits phosphatases to the LRRK2 complex. As such, phosphorylation levels of this residue have been used as a measure of LRRK2 kinase by type I kinase inhibitors.

These LRRK2 heterologous phosphorylation sites are targets of different phosphatases, such as Protein Phosphatase 1 (PP1) and Protein Phosphatase 2 (PP2) (Drouyer *et al.*, 2021).

3.3.2. LRRK2 in Parkinson's disease

The connection between LRRK2 and Parkinson's disease

In 2004, the *LRRK2* gene was identified as the gene responsible for the PARK8 locus. Mutations in *LRRK2* are a very common cause of familial PD, accounting for 4% of cases and causing a dominant form of the disease. GWAS analysis identified common genetic variants at the *LRRK2* locus as a risk factor for PD. Moreover, the symptoms of LRRK2 PD align with those for idiopathic PD, although some specific mutations present distinct phenotypes (Taymans *et al.*, 2023a). Importantly, it has been shown that LRRK2 interacts with many proteins known to be involved in PD, such as Tau, VPS35 and RAB29 (Usmani *et al.*, 2021). These findings provided further impetus for research in the involvement of *LRRK2* in PD, with the possibility of finding in the protein a therapeutic target.

PD-associated LRRK2 mutants and their pathological phenotypes

LRRK2 mutations responsible for familial PD cases comprise of missense mutations in the exons of the *LRRK2* gene. The most important alteration in the activity of PD-associated LRRK2 mutations is a hyperactivation of the kinase, leading to hyperphosphorylation of its targets. This is true for the majority of LRRK2 mutations that segregate with PD, and it has also been reported for some idiopathic PD cases (Goveas *et al.*, 2021). This is reflected by the fact that most of these mutations are localized within the catalytic core of LRRK2 (Soliman *et al.*, 2020). The prime example is LRRK2 G2019S, a missense mutation in KIN and one of the most common PD-associated LRRK2 mutation. Some of the phenotypes associated with these mutants include neurite shortening, a clear example of the importance of LRRK2 in the context of neurons, and destabilization of the cytoskeleton (Goveas *et al.*, 2021). The Tau protein interaction with microtubules stabilizes the structure, and this association is dependent on Tau phosphorylation levels. A hyperphosphorylated Tau detaches from the microtubule, destabilizing it and inducing Tau aggregation. Some PD-associated LRRK2 mutations, like R1441G in the ROC domain and I2020T in the KIN domain also show the characteristic phenotype of microtubule association. These mutations cause a conformational change that allows LRRK2 to associate with microtubules in an orderly manner (Tasegian *et al.*, 2021) affecting the activity of dynein and kinesin, altering transport in the cell.

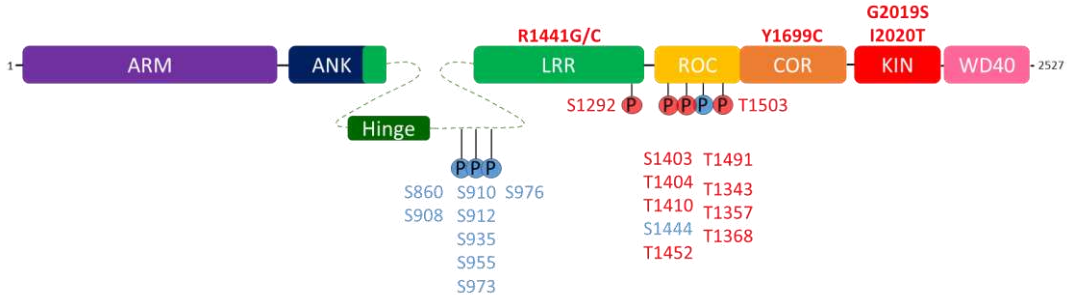

Figure 4 - ***PD associated LRRK2 mutations and LRRK2 phosphosites (Marchand et al., 2020)***
On top, some of the most important PD-associated LRRK2 mutations are represented at the level of the corresponding domain. On the bottom, notable phosphorylation sites are represented, with in blue heterophosphosites and in red autophosphorylation sites. The kinase domain closely regulates the GTPase activity via these autophosphosites.

LRRK2 kinase inhibitors and their role as a therapeutic strategy

Knowing the importance of LRRK2 kinase activity for PD, a direct approach to mediate the pathological functions of the protein in the disease is to inhibit said activity. Nowadays, LRRK2 kinase inhibitors constitute an important therapeutic strategy against LRRK2-PD phenotypes. There are currently two types of inhibitors. Type I kinase inhibitors compete with ATP for the ATP-binding pocket in the KIN domain (Tasegian *et al.*, 2021); an example of type I kinase inhibitor is MLi-2. Type II inhibitors similarly interact in the KIN domain, but to a region adjacent to ATP-binding pocket, maintaining it in an inactive state. Kinase inhibitors have been shown to effectively decrease the ability of LRRK2 to phosphorylate its targets. Importantly, treatment with type I inhibitors causes a reduction in phosphorylation of S935 as well, via the recruitment of phosphatases (Drouyer *et al.*, 2021). MLi-2 was also effective in inhibiting the activity of PD-associated LRRK2 mutants. The effectiveness of inhibitors, combined with the fact that many are brain-penetrant and can be orally ingested (Wojewska, Kortholt, 2021), have made them in the past a promising therapeutic strategy. However, kinase inhibitors can present some side effects. Similarly to some PD-associated mutants like R1441G LRRK2 and I2020T, treatment with MLi-2 induces LRRK2 oligomerization and microtubule association, a situation that may hinder organelle traffic along microtubes with catastrophic consequences for neurons, which heavily rely on long-range transport from the soma to the synaptic terminal (Tasegian *et al.*, 2021). Kinase inhibition is thought to also affect the levels of LRRK2, as LRRK2 phosphorylation is linked to the degradation of LRRK2 by the proteasome (Zhao *et al.*, 2015). Moreover, mice treated with MLi-2 show abnormal vacuolation in lung and kidney cells (Baptista *et al.*, 2020), although this effect is reversible once the inhibitor is withdrawn, and no lung degeneration. For these reasons, alternative strategies to regulate LRRK2 activity in PD need to be developed.

LRRK2 phosphorylation in PD

LRRK2 phosphorylation is highly modified in the context of PD. Two of the most studied phosphorylation phenotypes are the phosphorylation levels in the heterophosphorylation sites of the LRR cluster and at the autophosphorylation site serine 1292. The *SNpc* of PD patients is characterized by a reduced phosphorylation

of the LRR cluster (Marchand *et al.*, 2020) and transgenic rats expressing R1441C mutation present both an important deficit in motor functions and a drop in pS910 and pS935 levels in hippocampus. Conversely, the phosphorylation of S1292 is increased in mutants with a hyperactivated kinase activity, like G2019S. It is possible that the phosphorylation levels of LRRK2 in specific sites directly affects LRRK2 catalytic activity, and has therefore an important role in PD. To test this, the effect of dephosphorylation can be studied by mutating commonly phosphorylated serine into alanine residues. Alanine is biochemically very similar to serine, but it lacks the hydroxyl group necessary for phosphorylation to occur. Mutants from serine to alanine are therefore called phosphodead mutants. Research testing LRRK2 kinase activity via *in vitro* kinase assays found the LRRK2 phosphomutants in the LRR hotspot to have a general tendency to increase kinase activity (Reynolds *et al.*, 2014). Moreover, when overexpressing RAB29 in the presence of either LRRK2 WT or LRRK2 phosphomutants, the LRRK2 phosphodead mutants show a much stronger increase in kinase activity than the WT (Marchand *et al.*, 2022). Another useful tool is provided by phosphomimetic mutants. In this case, serine is substituted with aspartic acid, which resembles phosphorylated serine for the presence of both a negative charge on both amino acids at physiological pH, and a double bond on an oxygen atom (*figure 7*). Furthermore, phosphorylated serine and aspartic acid have similar steric incumbrance, important in determining the local structure of a protein. Because of this, it is possible that a phosphomutant LRRK2 from serine to aspartic acid could behave like a constitutively phosphorylated LRRK2 protein. Interestingly, kinase activity assays show that phosphomimetic mutants present decreased kinase activity (Marchand *et al.*, 2022). Taken together, these findings suggest that the phosphorylation levels on the LRR hotspot can influence kinase activity and more specifically that preserving phosphorylation can decrease LRRK2 kinase activity. The mechanism behind the relationship between phosphorylation and kinase activity is still not clear, but this evidence suggests that protection of phosphorylation on the LRR hotspot would have a beneficial effect in PD. In search of effective methods to protect phosphorylation, researchers have studied what are the proteins interacting with LRRK2 at this hotspot. Importantly, it was shown that some of the LRR-ANK phosphodead mutants lose the ability to interact with the 14-3-3 protein (Marchand *et al.*, 2020).

3.4. The 14-3-3 protein: a modulator of LRRK2 in Parkinson's disease

3.4.1 General knowledge

Brief historical overview

The 14-3-3 protein it was discovered by Moore and Perez in 1967 via the purification of proteins in bovine brain tissue (Morrison, 2008). The genes for the 14-3-3 family are ubiquitous in eukaryotic species and cells, with a high degree of conservation, and in mammals the highest expression level is reached in the brain.

This suggested an important role in cellular homeostasis. Research over the years has validated the role of the 14-3-3 family as adaptors and chaperones for many different proteins, playing important roles in cell growth, apoptotic suppression and neurodegenerative diseases.

Protein family and structure

14-3-3 proteins are small acidic proteins, ranging from 27 to 29 kDa, found in the cytosol. In mammals, seven isoforms, with slight differences in sequence are recognized: *β, γ, ε, ζ, σ, η* and *θ* (Morrison, 2009). All these isoforms are encoded by different genes (Obsilova, Obsil, 2022). Additionally, 14-3-3 monomers cannot perform their function alone, but instead 14-3-3 proteins work in the form of dimers, which can be either homodimers of the same isoform or heterodimers. Nowadays, there is no clear idea on the specific function of each isoform; however, said isoforms do show distinct affinity for proteins (Obsilova, Obsil, 2022) and even specific expression patterns in the body (Paul *et al.*, 2012) (*table 4*). Each monomer is formed by nine alpha helices in antiparallel order and when forming the dimer, the two monomers arrange themselves in W-shape (Ballone *et al.*, 2018). In this conformation, the concave surface forms, on each monomer, an amphipathic groove, surrounded by one end charged polar residues and on the other hydrophobic residues (*figure 5*). Isoforms differ in the amino acids that constitutes the dimer interface (Paul *et al.*, 2012), which affects their ability to create these dimers. This is also the reason why 14-3-3 σ only creates homodimers and has a more specific array of interactors (Paul *et al.*, 2012).

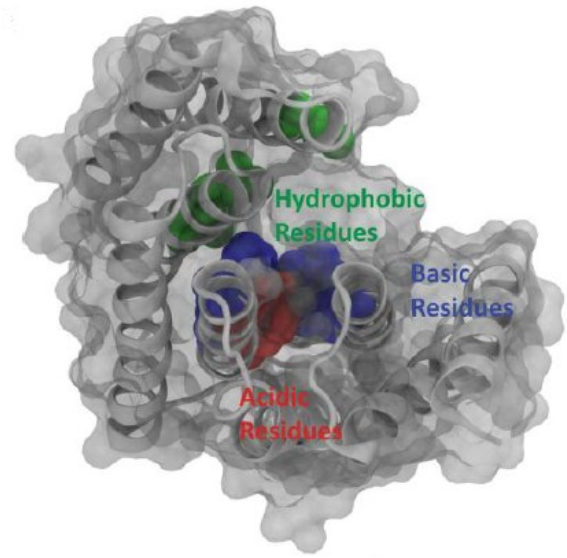

Figure 5 - View of the 14-3-3ζ monomer (Ballone et al., 2018)
Acidic, basic and hydrophobic residues that define the amphipathic groove are respectively shown in red, blue and green. This groove is responsible for the phosphorylation-dependent recognition of the target.

Table 4 – 14-3-3 isoforms (uniprot, Paul et al., 2012)		
Isoform	**Size (kDa)**	**Important sites of expression**
β	28.082	Middle temporal gyrus, substantia nigra pars compacta
γ	28.303	substantia nigra pars compacta, main isoform in hippocampus
ε	29.174	Superior frontal gyrus, ventricular zone
ζ	27.745	Oral epithelium
η	28.219	Frontal pole
θ	27.764	Sperm, endothelial cells
σ	27.774	Cervix squamous epithelium, only expressed in epithelial cells

14-3-3 as modulators

14-3-3 proteins have a fundamental role as modulators for the activity of their targets. This is achieved through a direct interaction between the 14-3-3 dimer and its target, forming a new complex. The ways in which this new complex formation modulates the ligand's activity vary significantly, depending on the ligand in question. 14-3-3 proteins can sterically hinder the interaction between the ligand and other proteins, or, on the contrary, favour said interaction by autorecognition (Pennington *et al.*, 2018). It can alter the structure of the ligand or impede a conformational change, and its presence can mask important sequences in the protein, altering its localization. A fundamental cellular process in which the 14-3-3 proteins fulfil their role as regulators is cell cycle. It has been shown that most 14-3-3 proteins act as an anti-apoptotic agent, by preventing the shuttling of transcription factors, such as Foxo3a and Bax, to the nucleus (Kaplan *et al.*, 2017). Because of this, 14-3-3 family members are considered growth promoters in the context of cancer, with the exception of 14-3-3 *δ*, which is considered a tumour suppressor.

3.4.2. 14-3-3 protein-protein interaction

Interaction between 14-3-3 and its target depends on the phosphorylation of serine or threonine residues on the target that are often present in disordered regions of the target (Stevers *et al.*, 2018) and usually occurs in pairs. This localization of the residues allows that 14-3-3 monomer can independently bind one of the two phosphorylated residues (Shen *et al.*, 2003), which increases the affinity of the target protein and stabilizes the complex. This also explains why, for some 14-3-3 targets, the monomeric form of the adaptor protein is sufficient to form the complex. This interaction would be likely mediated by a high-affinity site on the target (Shen

et al., 2003). Additionally, when two residues are needed, the phosphorylation of these amino acids can be regulated via different pathways, indicating the importance of 14-3-3 proteins in the proper integration of different signalling cascades.

14-3-3 protein-protein interaction as a drug target

14-3-3 interactions with their targets can be either inhibited or strengthened, using different molecules or peptides. For weakening the bond, a common strategy is to use the R18 peptide, which interacts with the 14-3-3 groove and blocks it from entering in contact with its targets (Cao *et al.*, 2009). An R18 derived tandem sequence has also been developed, called "dimeric fourteen-three-three peptide inhibitor' or difopein, a commonly used general inhibitor for 14-3-3, inhibiting all interactions between the protein and its targets (Cao *et al.*, 2009). Studies have shown that difopein expression induces apoptosis in cells and reduces tumour growth in mice (Cao *et al.*, 2009).

For strengthening the bond between 14-3-3 and its target, a strategy involves the use of bivalent molecules, composed of two independent groups, able to interact with the two targets, and a linker connecting them. While this is in fact effective, a major problem in the application of these compounds as drugs is their size, which hinders the ability of the molecule to easily solubilize, important for oral drugs (Wu *et al.*, 2022). A newer approach involves the use of molecular glues, a small type of molecule that takes advantage of the secondary structure of the proteins involved. A molecular glue will interact with one of the proteins, changing its local conformation to create a binding region for the second protein (Wu *et al.*, 2022). Their small size allows for high solubility and thus better uptake and the possibility of oral treatments development. Moreover, they can be designed for specific interactions, which is crucial when talking about 14-3-3 and its many different targets. There are already available molecular glues for 14-3-3, like fusicoccins, a class of compounds discovered in fungi (Wu *et al.*, 2022). These natural compounds bind to a pocket created by the interface of the 14-3-3 groove and the ligand's motif that is recognized by 14-3-3. They strengthen the bond between the two proteins, without competing for the 14-3-3 groove with the ligands.

3.4.3. The LRRK2:14-3-3 complex in Parkinson's disease

14-3-3 and Parkinson's disease

The relationship between the 14-3-3 proteins and PD has been an important field of study for many years. It has been shown that 14-3-3 expression is reduced in mouse models of PD (Kaplan *et al.*, 2017), and some 14-3-3 isoforms can be found in Lewy Bodies. 14-3-3 overexpression can revert the cellular phenotypes associated with PD such as neurite shortening, while expression of difopein exacerbates such phenotypes. These findings suggest that 14-3-3 proteins play a vital role in PD, by modulating other proteins involved through the formation of the 14-3-3:protein complex. Important proteins known for their role in PD were demonstrated to be able to interact with 14-3-3 proteins. An example of this in α-synuclein (Giusto *et al.*, 2021), where the interaction with 14-3-3 proteins is thought to impede cell-to-cell transmission of the pathologic version of the protein. Parkin, a protein involved

in the degradation of misfolded proteins, interacts with both α-synuclein and 14-3-3, and co-localizes with 14-3-3 at Lewy bodies (Giusto *et al.*, 2021). Importantly, 14-3-3 forms a complex with LRRK2, modulating its activity and subcellular localization.

14-3-3 interacts with LRRK2

Researchers have found that LRRK2 is one of the targets of the 14-3-3 proteins. In fact, 6 out of the seven isoforms of 14-3-3 are able to interact with different affinity, with the exception of 14-3-3 δ, which does not interact at all (Nichols *et al.*, 2010; Manschwetus *et al.*, 2020). 14-3-3 isoforms have been reported to recognize LRRK2 on the disordered region close to the N-terminus of LRR, the same region where the heterophosphosites cluster is found. In fact, the formation of the LRRK2:14-3-3 complex is dependent on the phosphorylation of serine 910 and serine 935, since the mutation of serine to alanine on S910A and S935A LRRK2 abolishes interaction with 14-3-3 proteins (Nichols *et al.*, 2010). However, not much is known about the 3D structure of the LRRK2:14-3-3 complex, as the binding motif on LRRK2 is, similarly to other ligands of 14-3-3, disordered in nature. This makes it difficult to study the complex with classical techniques, such as X-ray crystallography (Somsen *et al.*, 2022), so most studies use synthetic phosphopeptides as a surrogate for the entire protein (*figure 6*).

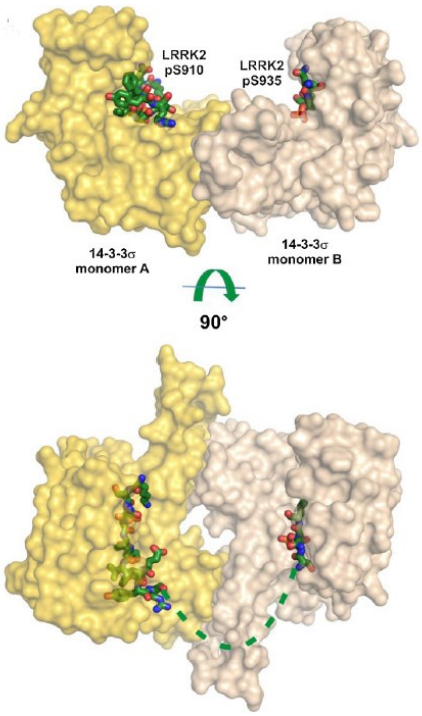

Figure 6 - Crystal structure of 14-3-3 σ monomers (protomers) with LRRK2 peptides (Kaplan et al., 2017)
The LRRK2 phosphorylated peptides show the position of the amphipathic groove in the 14-3-3 protein. The green dotted line represents the linker region that connects S910 and S935, which is not visible in the electron density obtained by the X-ray crystallography.

14-3-3 binding to LRRK2 influences phosphorylation levels at S910 and S935

After determining the presence in cells of the LRRK2:14-3-3 complex, researchers moved on to determine whether this complex was involved in PD. Several pieces of evidence support this idea. First, PD-associated LRRK2 mutants, like LRRK2 R1441G, Y1699C, I2020T, and, to a lesser extent, G2019S, show a decreased ability to form the LRRK2:14-3-3 complex, as well as a decrease in the phosphorylation of serine 910 and serine 935 (Nichols *et al.*, 2010). Experiments *in vitro* and *in vivo* show that overexpression of 14-3-3 θ can increase the phosphorylation levels at these heterophosphosites; on the contrary, difopein expression significantly reduces the LRRK2 S910 and S935 phosphorylation levels (Lavalley *et al.*, 2016). Most importantly, similar results were observed when testing the phosphorylation of LRRK2 WT, but also of LRRK2 G2019S, proving that 14-3-3 overexpression can affect PD-associated LRRK2 mutants.

14-3-3 binding keeps LRRK2 in a monomeric cytosolic form

An important way in which 14-3-3 proteins modulate their target's activity is by altering its subcellular localization. In the case of LRRK2, it was shown that 14-3-3 maintains LRRK2 in a monomeric cytosolic form (Marchand *et al.*, 2022). This is relevant, because of the increase in kinase activity that LRRK2 experiences when it dimerizes at the level of membranes. Studies have shown that LRRK2 phosphomutants S910A and S935A, unable to form the complex with 14-3-3, tend to accumulate in cytosolic pools (Nichols *et al.*, 2010).

14-3-3 binding decreases kinase activity in PD-associated LRRK2 mutants

Given the importance of LRRK2 kinase hyperactivity in PD, one can wonder whether this PD phenotype is affected by the formation of the LRRK2:14-3-3 complex. When overexpressed in WT or G2019S LRRK2 cells, 14-3-3 θ induces a reduction in S1292 phosphorylation levels, a common readout of kinase activity (Lavallaey *et al.*, 2016). This effect, however, is lost when the serines 910 and 935 are mutated into alanines, proving that 14-3-3's effect on kinase activity is mediated by its ability to create the LRRK2:14-3-3 complex.

14-3-3 reverts cellular phenotypes of G2019S LRRK2

The positive effect of 14-3-3 expression is not limited to molecular readouts. In fact, 14-3-3 θ overexpression in cells expressing G2019S LRRK2 reverts the neurite length deficits bringing neurite length back to physiological levels. On the contrary, the expression of difopein exacerbates this phenotype (Lavalley *et al.*, 2016).

3.4.4. The LRRK2:14-3-3 complex, a possible drug target?

To recapitulate, the LRRK2 protein plays an important role in PD, presenting an increased kinase activity and a dephosphorylation at serines 910/935 as PD-associated phenotypes. 14-3-3 binds LRRK2 when these two serines are phosphorylated and maintains that phosphorylation. Moreover, the adaptor protein has a neuroprotective effect in LRRK2-PD that depends on the formation of this complex.

4. Objectives

Research on LRRK2 has shown that the protein is a promising potential therapeutic target for PD. Evidence supporting it is multiple, spanning from the genetics of both monogenic and idiopathic forms of PD, to the identification of molecular LRRK2 phenotypes associated with PD, most importantly the increased kinase activity. Accumulating evidence indicates that have also found in the phosphorylation of LRRK2 represents an important way whereby both the protein's activity and its interaction with other proteins are affected. Most importantly, the 14-3-3 proteins were confirmed as key LRRK2 interactor, capable of positively affecting phenotypes associated with LRRK2 PD, and this interaction depends on the phosphorylation of key heterophosphosites, including serine 910 and serine 935. 14-3-3 overexpression was shown to negatively affect LRRK2 kinase activity readouts, suggesting that the modulator protein is capable of maintaining LRRK2 in a less active state. Moreover, 14-3-3 overexpression was also shown to positively affect cellular phenotypes of PD-associated LRRK2 mutants. **Considering these results, our working hypothesis is that strengthening the association between LRRK2 and 14-3-3 can have a beneficial effect in the context of PD.** This work focuses on determining phenotypes of the LRRK2:14-3-3 complex in various conditions and with different techniques. To achieve this, various conditions were tested, including 14-3-3ζ, difopein and difopein mutant overexpression.

Specific objective 1: LRRK2 phosphomutants are tested to also determine their viability as negative and positive controls of the LRRK2:14-3-3 complex formation. One of these mutants is the phosphodead mutant LRRK2 6xS>A (*figure 7*), where multiple serines of the LRR cluster known to be heterophosphosites have been mutated into alanine. This LRRK2 mutant could then be used as a negative control for the LRRK2:14-3-3 interaction, since 14-3-3 would be unable to interact without the presence of phosphorylated serines. On the contrary, the LRRK2 6xS>D phosphomutant is designed to be a possible positive control of the interaction, as the aspartic acid side chain approximates in charge and steric incumbrance a phosphorylated serine (*figure 7*).

Specific objective 2: it is known that type I LRRK2 kinase inhibitors induce a dephosphorylation of the LRR cluster heterophosphosites. One hypothesis is that the kinase inhibitors affect the LRRK2 structure in such a way that phosphatases are recruited to LRR cluster, causing dephosphorylation. Knowing that 14-3-3 proteins overexpression causes an increased phosphorylation levels in the LRR cluster, it is possible that 14-3-3 shields the heterophosphosites from phosphatase activity. 14-3-3 overexpression would then be able to modulate the sensitivity of LRRK2 to type I kinase inhibitors, so that higher concentrations of inhibitor are required to achieve dephosphorylation. Using phosphorylation of serine 935 as a readout, the effect of 14-3-3 overexpression and difopein expression on kinase inhibitor treatment are here tested for any effect on LRRK2 sensitivity to the inhibitor.

Specific objective 3: LRRK2 subcellular localization can be affected by different factors, causing specific phenotypes like microtubule association caused by type I

kinase inhibitors. Interestingly, phosphodead mutants show a particular phenotype where LRRK2 accumulates in cytosolic pools. Considering that there is evidence that 14-3-3 maintains LRRK2 diffused in the cytosol, LRRK2 subcellular localization under various conditions affecting 14-3-3 will be explored. The interaction between 14-3-3 overexpression and kinase inhibitor treatment is studied, to test whether 14-3-3 is able to reestablish the diffused phenotype instead of microtubule association.

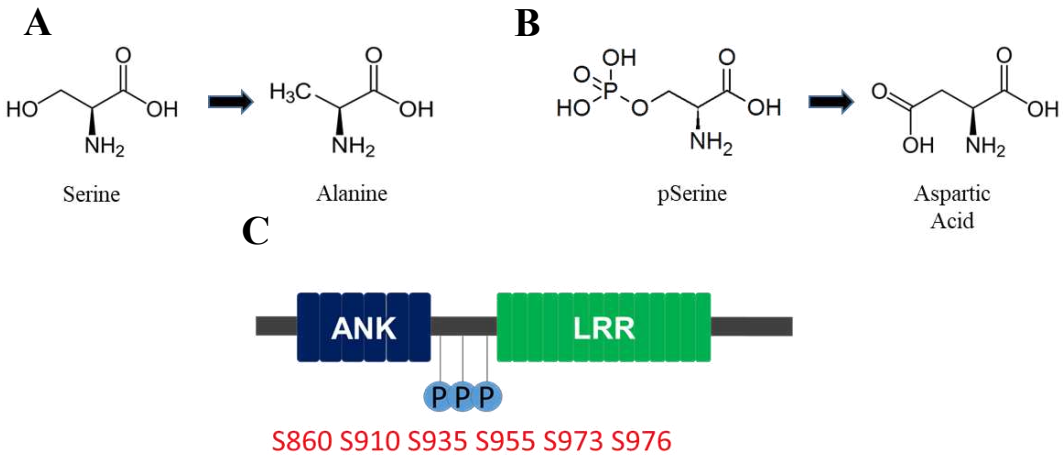

Figure 7 - LRRK2 phosphomutants
(A) *The comparison between the amino acids serine and alanine is presented, showing the close resemblance between the two molecules, except for the hydroxylic group on serine, necessary for the bond with a phosphate group.* ***(B)*** *The comparison between the amino acids serine and aspartic acid is presented, showing the resemblance in overall charge and size.* ***(C)*** *The serines mutated in the LRRK2 6xS>A and LRRK2 6xS>D mutants are depicted.*

5. Materials and methods

5.1. Plasmids

5.1.1. List of plasmids

The plasmids coding for LRRK2 used in this work consisted of transfer plasmids based on the pLV-CSJ backbone (an in-house lentiviral vector backbone generated by Dr. Taymans of Lille Neuroscience & Cognition) containing the LRRK2 variants of interest and resistance marker for ampicillin. The 6xS>A and 6xS>D indicate the mutations of 6 serines (S860, S910, S935, S955, S973, S976) to either alanine or aspartate. These plasmids were available in the lab in Lille (Marchand *et al.*, 2020; Marchand *et al.*, 2022). The plasmids coding for difopein, available in a modified peGFP-C1 backbone, with kanamycin resistance marker were made available by the laboratory of Prof. Greggio at the University of Padova. The list of plasmids is the following (*table 5)*:

Table 5- plasmids utilized

Plasmid	Antibiotic resistance
pLV-CSJ	Ampicillin
pLV-CSJ-3xFlag-LRRK2 WT	Ampicillin
pLV-CSJ-3xFlag-LRRK2 S910A	Ampicillin
pLV-CSJ-3xFlag-LRRK2 S935A	Ampicillin
pLV-CSJ-3xFlag-LRRK2 S955A	Ampicillin
pLV-CSJ-3xFlag-LRRK2 S973A	Ampicillin
pLV-CSJ-3xFlag-LRRK2 6xS>A	Ampicillin
pLV-CSJ-3xFlag-LRRK2 6xS>D	Ampicillin
pCMV-3B-2xMyc-14-3-3	Kanamycin
pSCM138-eYFP-difopein	Kanamycin
pSCM174-eYFP-R18 D12K E14K	Kanamycin

5.1.2. Bacteria transformation

Petri dishes were prepared with Lysogeny broth (LB) agar (Sigma-Aldrich, L3022), solubilized in hot Mili-Q water, and complemented with either 100 µg/mL of ampicillin (Sigma-Aldrich, A9518) or 50 µg/mL of kanamycin (Sigma-Aldrich, K4000). The LB agar was left to solidify. To prepare the needed plasmids, competent *E.coli* cells of the DH5-α strain (Invitrogen, 18263-012) was used. First, 50 µL of DH5-α cells kept at -80 °C were defrosted on ice for at least 15 minutes. Once completely defrosted, 100 ng of the desired plasmid were gently mixed with the bacteria, and the resulting mix was left on ice for 10 minutes. After this, heat-

shock was performed with first 45 seconds in a 42 °C water bath, followed by 3 minutes on ice. 200 µL of LB medium were added to the bacteria, and the resulting mix was incubated 45 minutes at 37 °C in oscillation 120 rotations per minute (RPM). The resulting solution was seeded on the proper petri dish and left to incubate overnight at 37 °C.

5.1.3. Plasmid amplification and purification

To amplify plasmids, a single transformed colony from the Petri dish was picked and added to 200 mL of LB medium, with either 100 µg/mL of ampicillin (Sigma-Aldrich, A9518) or 50 µg/mL of kanamycin (Sigma-Aldrich, K4000). The culture was then left to incubate overnight at 37 °C in oscillation at 120 RPM. The amplified plasmid was purified using the PureYield Plasmid Midiprep System (Promega, A2495), yielding purified plasmid in 400 µL of nuclease-free water. Double strand DNA concentration was measured via Nanodrop (ThermoFisher Scientific, USA).

5.2. Cell culture

For the following experiments, Human Embryonic Kidney (HEK293T, ATCC, CRL-3126) were used. Cells were cultivated with full medium, prepared with high-glucose medium Dulbecco's Modified Eagle Medium (DMEM, Sigma Aldrich, D6429) and supplemented with:

- 100 U/mL of penicillin and 100 µg/mL of streptomycin (Fischer Scientific, 15140122)
- 10% Fetal Bovine Serum (Gibco, A3160801)
- Non-essential amino acids (Gibco, 11140-035)

Cells were maintained in T75 flasks in a constant humid atmosphere of 37 °C, 5% CO_2. Passaging was performed twice a week when confluency of the flask was reached, at around 8.4 x 10^6 cells. First, the old medium was removed, and the flask was gently washed with 5 mL Dulbecco's Phosphate Buffered Saline (PBS, Sigma Aldrich, D8537). Next, 2 mL of PBS 0.05% Trypsin-EDTA (Gibco, 15400-054) were added to the flask, which was then put to incubate at 37 ºC for 2 minutes. 8 mL of fresh full medium were added, thoroughly mixing to resuspend cells by re-pipetting multiple times, making sure to detach the cells from the culture vessel's surface. Of this resuspension, 1 mL was used to seed a new T75 flask, performing a 1:10 passage. 9 mL of fresh full medium were then added to the flask, which was again put to incubate. Cell seeding onto different plates was performed by resuspending cells from the maintenance flask using the same method as cell passage. For each of the different supports used, the volume of resuspension of cells from the T75 maintenance flask was calculated by multiplying the ratio of the desired passage (1:10) with the ratio of the used culture vessels' surface areas (receiving vessel surface/T75 flask surface). The culture vessels used for the purpose of the experiments were, in descending order of surface area: 10 cm dishes

(56.7 cm^2), 6-well plates (9.6 cm^2), 12-well plates (3.5 cm^2), 24 well plates (1.9 cm^2).

5.3. Transfection

Transfection was performed using the same procedure and transfection reagent for all experiments, adjusting the volumes depending on the culture vessel on which cells were grown. For cells grown in 10 cm plates, transfection was performed as follows:

1. Cells were allowed to grow until 80% of confluency is reached
2. Old medium was changed with fresh full medium no later than 30 minutes before transfection, possibly 8 hours before
3. Plasmids were added to an Eppendorf with 500 µL of pure DMEM. For plasmids of bigger size (i.e., LRRK2) constructs, 12 µg were used. For smaller sized plasmids (i.e., 14-3-3/difopein/difopein scrambled), 2 µg were used.
4. DMEM + DNA was vortexed to homogenize the solution
5. In another Eppendorf with 500 µL per each condition, LipoD293 transfection reagent (SignaGen Laboratories, SL100668) was added with a ratio of 3:1 (LipoD:DNA), meaning that for each µg of DNA to be transfected, 3 µL of LipoD293 reagent were added
6. The Eppendorf with LipoD293 was vortexed and left to incubate 3 minutes at room temperature
7. 500 µL of DMEM + LipoD293 was added to the 500 µL of DMEM + DNA, making sure that the DMEM + LipoD293 was placed on top of DMEM + DNA
8. The Eppendorf was vortexed and left to incubate 10 minutes at room temperature
9. The final solution of 1000 µL was added dropwise on top of the cells, covering as much surface area as possible to guarantee equal transfection
10. New change of medium is performed with fresh full medium after 8 hours
11. At around 40 to 48 hours post-transfection, the cells were considered ready to use in the experiments

For 6-well plates and 12-well plates, the protocol remains identical, except for the dose of reagents used. For 6-well plates, 2 µg of DNA were used for LRRK2 plasmids, while for the other plasmids 300 ng of DNA were used, in a total volume of 200 µL. For 12-well plates, 1 µg of LRRK2 DNA 100 ng of DNA for the other plasmids were used, in a total volume of 100 µL. When some conditions required

co-transfection, those that did not were co-transfected anyway, using the empty backbone pLV-CSJ, to maintain equal transfection conditions.

5.4. Pharmacological treatment

Treatment with MLi-2 inhibitor was performed by changing old used cell medium with fresh medium containing MLi-2 (Tocris, 5756) in dimethyl sulfoxide (DMSO) (Sigma Aldrich, D4540). After 1 hour, the medium was removed, completing the treatment. MLi-2 was added to the fresh medium at various concentrations, depending on the sample and experiment.

5.5. Cell collection, lysis and BCA protein assay

5.5.1. Collection

10 cm dishes

Cell collection was performed by removing the old medium, gently washing with 2 mL of Dulbecco's PBS, and incubating with 2 mL 0.05% trypsin-EDTA for 2 min. After this, 6 mL of Dulbecco's PBS were added, and cells were collected by gently pipetting up and down with a 5 mL pipette in 14 mL tubes. The tubes were then centrifuged at 1000 relative centrifugal field (rcf) for 6 minutes at 4 °C, discarding the supernatant and keeping the obtained pellet on ice.

24-well plates

Cell collection was performed by removing the old medium, and directly adding 1 mL of cold Dulbecco's PBS in each well. Through vigorous pipetting, cells were detached and transferred to 1.5 mL Eppendorfs. Plates were kept on ice throughout the process. The Eppendorfs were centrifuged at 1000 rcf for 6 minutes at room temperature, discarding the supernatant and keeping the obtained pellet on ice.

5.5.2. Lysis

Pellets of cells obtained through collection were then resuspended in ice-cold lysis buffer [20 mM Tris pH 7.5, 150 mM NaCl, 0.2% TritonX-100, 5 mM $MgCl_2$, 10% glycerol, protease inhibitor (Sigma-Aldrich, 046931320019 and phosphatase inhibitor (Sigma-Aldrich 4906837001)]. For cells coming from 10 cm dishes, 1 mL of lysis buffer was used, and for cells coming from 24 well plates, 100 µL were used. Lysis was performed for 30 minutes at 4 °C in rotation. After this, samples were centrifuged at 15000 rcf for 15 minutes at 4 °C, and the resulting supernatant was kept.

5.5.3. BCA protein assay

Protein levels in samples were assessed using a bicinchoninic acid assay (BCA) kit (ThermoFisher Scientific, 23227). To properly analyze protein concentration, the bovine serum albumin (BSA) standards included in the kit were used, and all samples were prepared in duplicate. Protein samples coming from experiments were diluted 1:5 using lysis buffer.

5.6. Co-Immunoprecipitation, Western Blot and Dotblot

5.6.1. Co-Immunoprecipitation

Co-Immunoprecipitation was performed on samples coming from 10 cm dishes. 50 µL were set aside to be used as input, while the rest of the lysate was put to incubate with 15 µL of anti-FLAG M2 magnetic beads (Millipore, M8823) for 2 hours at 4 °C in rotation. These beads allowed to easily capture of FLAG-tagged proteins (LRRK2) and their complexes via the use of anti-FLAG M2 antibody attached to magnetic beads. After incubation, samples were washed 3 times with lysis buffer, avoiding the loss of the proteins of interest via magnetic stands. 30 µL of a solution of 2X LDS (Invitrogen, NP007) and reducing agent (Invitrogen, B0009) were added to each sample, followed by vortex, heat treatment at 95 °C for 10 minutes and another vortex. These steps allowed to detach the proteins of interest, alongside the antibodies used for capture, from the magnetic beads.

5.6.2. Western Blot

Gel electrophoresis

Samples destined for western blot were prepared by mixing 3.5 µL of 2.85X LDS with reducing agent, the volume of cell lysate necessary to have 15 µg of total protein, and a volume of PBS calculated to reach 10 µL in total. The prepared dilutions were boiled at 95 °C for 5 minutes, to assure complete denaturalization of proteins for proper electrophoresis. Electrophoresis was performed using 4-12% Bis-Tris NuPAGE precast gels (Invitrogen, NP0329) with 1X MOPS running buffer (Invitrogen, NP0001). Samples were run at 100 V for 1h30, until the first 10 kDa and 15 kDa bands have run out completely.

Membrane transfer

After proper electrophoresis, the proteins, now separated by weight, were transferred onto Nitrocellulose membranes of thickness 0.45 µm (Cytiva, 10600002). Transfer was performed at 40 mA overnight at 4 °C, using transfer buffer (20 mM Tris pH 8.6, 122 mM glycine, 5% MeOH).

Blocking, antibody incubation and visualization

After transfer, membranes were stained with Red Poinceau (Sigma-Aldrich, P7170) to verify proper transference and aid in membrane cutting. Membranes were cut to blot the proteins of interest with different antibodies. Blocking was performed for 1 hour at room temperature, using 5% BSA (EMD Millipore, 12659) (w/v) in 0.1 % PBS-Tween20. After blocking, membranes were incubated with primary antibodies (*table 4*), diluted in the same blocking solution, overnight at 4 °C in lateral oscillation 60 RPM. The day after, the diluted antibodies were kept for later uses, and membranes were washed 3 times with 0.1 % PBS-Tween20 for 10 minutes. Incubation with HRP-conjugated secondary antibodies (*table 5*), diluted in 0.1% PBS-Tween20, was then performed for 1 hour at room temperature. The same washing steps was re-performed, and membranes were incubated with ECL standard (Cytiva, RPN2209) or ECL prime (Cytiva, RPN2236) for 1 minute, and the chemiluminescent reaction was detected with either Imager600 or Imager800 (GE Healthcare, USA).

5.6.3. Dotblot

The dotblot technique is a high-throughput, low-tech and cost-effective method to capture proteins onto a membrane in order to perform immunodetection. It uses a specific bio-dot apparatus (*figure 8*) that, through a vacuum, pulls cell lysates through the membrane, without the need for electrophoresis or protein transfer from the membrane to the gel. For the dotblot protocol, Nitrocellulose membranes of thickness 0.45 µm (Cytiva, 10600002) and whatman filter papers (WHA1001090) were wet with Dulbecco's PBS and mounted into the apparatus, with the nitrocellulose membranes placed on top of the whatman filter paper. 50 µL of PBS were then loaded into the apparatus' wells, followed by 30 µg of cell lysates for each sample. Vacuum was applied to the apparatus for 1 minute after the complete passing of liquid through the membrane. The obtained membrane was submitted to the same immunodetection procedure as described for Western Blot experiments and treated the same way until final visualization.

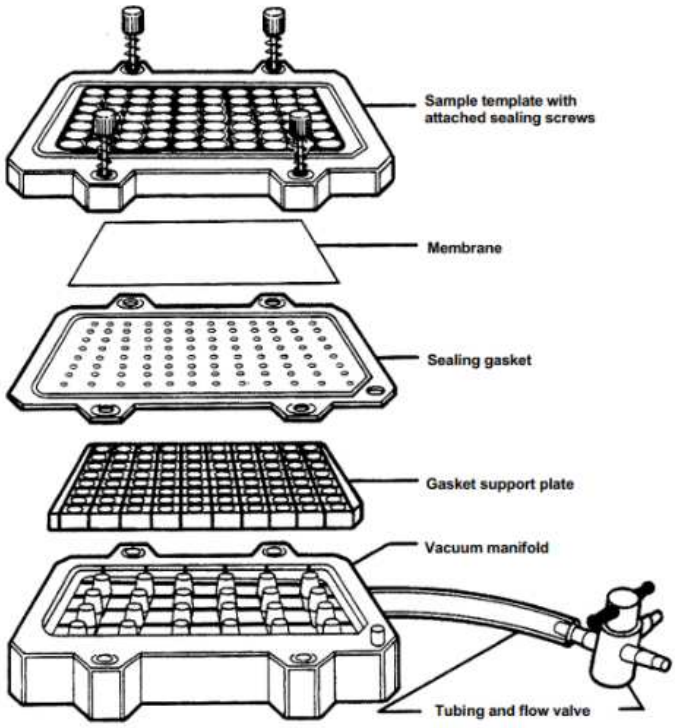

Figure 8 - Bio-dot apparatus (Biorad, 1706545). The sample template presents 96 separated wells where samples can be loaded. Once the vacuum is applied, the liquid gets collected in the manifold and the proteins fix on the membrane.

5.6.4. Signal quantification and analysis

Signal coming from western blots and dotblots was quantified using the Image Studio software, which gives densitometry data that then can be used for statistical analysis. For statistical analysis of densitometry data of all blots, each condition was normalized over the corresponding control. For experiments testing levels of phosphorylated S935 LRRK2, two blots were prepared for each sample, one for total LRRK2, and one for phosphorylated serine 935 (pS935) LRRK2. The obtained densitometry data was used to calculate the ratio pS935 LRRK2/total LRRK2. To

analyse the dose range data and to correctly compare samples from different biological replicates, a different mathematical calibrator for each replicate was prepared. This was achieved by summing up all the pS935/total LRRK2 ratios of the samples making up the dose-response curve of the control specific to that biological replicate. The mathematical calibrator was then used to normalize the ratios of the dose-response curves of the studied conditions.

5.7. Immunocytochemistry

The immunocytochemistry experiment was performed by first transfecting cells in 12-well plates. In another 12-well plate, coverslips were prepared by adding 100 µL of Poly-D-Lysine (Sigma Aldrich, P0899) for 5 minutes, to guarantee better cell adherence to the cover slips. Instead of a simple change of medium, cells were passaged from the old 12-well plate to the new one at a 1:6 passage. This permits optimal cell spreading, without overcrowding the coverslip with cells. The next day, the medium was removed, and cells were treated for 15 minutes with 500 µL of 4% paraformaldehyde (PFA) in PBS. PFA was then removed, and cell were permeabilized with 1 mL of PBS with TritonX-100 at 0.2% for 10 minutes at room temperature with gentle lateral rocking at 30 RPM, and transferred to a 24-well plate. Blocking was performed for 1 hour at room temperature in gentle rocking at 30 RPM, using 0.5% BSA (w/v) in PBS with TritonX-100 at 0.2%. The coverslips were put to incubate with 100 µL of the primary antibodies, diluted in the same blocking solution, overnight at 4 °C in gentle rocking at 30 RPM. The next day, two washes with PBS with TritonX-100 at 0.2% were performed for 10 minutes at room temperature in oscillation, and 100 µL of the secondary antibodies, diluted in the same washing solution, were added to each well. Incubation was performed for 1 hour at room temperature in gentle rocking at 30 RPM, making sure to keep the coverslips protected from light. After two additional washes, the coverslips were left to air-dry at room temperature in the dark for 30 minutes. Finally, the coverslips were mounted on microscope slides, using 3 µL of Vectashiled mounting medium with DAPI (Vector Laboratories, H-1200).

Imaging and analysis

For determination of the percentage of cells displaying filamentous localization of LRRK2, cells were visualized on an inverted microscope (Zeiss AxioImager) using a 100X 1.4 Plan APO oil objective. Scoring was performed via live imaging, while representative pictures were taken by preparing a Z-stack of 7-10 slices of 0.5 µm. Camera exposure was adjusted according to the emitted signal for each channel of each condition. For coverslip, around 80 random cells were scored for LRRK2 subcellular localization (cytosolic, punctate, filamentous, amorphous). Quantification of the subcellular localization was performed blind to condition.

5.8. Antibodies

Primary (*table 6*) and secondary (*table 7*) antibodies were used in western blots, dotblots and immunocytochemistry (ICC) experiments (*table 4)*. For western blot and dotblots, secondary antibodies were conjugated with Horse Radish Peroxidase (HRP), able to produce light when ECL substrate is provided. For ICC, secondary antibodies conjugated with Alexa Fluor dyes.

Table 6 – Primary Antibodies

Antibody name	Reference	Species	Dilution
Anti-FLAG M2	**Sigma Aldrich** F1804-200UG	Mouse	1:500
Anti-Hsp90	**BD Biosciences** 610418	Mouse	1:1000
Anti-Myc tag	**Millipore** 05-724	Mouse	1:2000 (Western Blot) 1:500 (ICC)
Anti-α-Tubulin	**Novus Biologicals** NB100-690	Mouse	1:10000
Anti-pS935 LRRK2	**Abcam** ab133450	Rabbit	1:1000
Anti-LRRK2	**Abcam** ab133518	Rabbit	1:200

Table 7 – Secondary Antibodies

Antibody name	Reference	Species	Dilution
Anti-mouse IgG-HRP	**Cell Signaling technology** 7076S	Mouse	1:10000
Anti-rabbit IgG-HRP	**Cell Signaling technology** 7074S	Rabbit	1:5000
Anti-mouse IgG-AlexaFluor 488	**ThermoFisher Scientific** A11001	Donkey	1:1000
Anti-rabbit IgG-AlexaFluor 568	**ThermoFisher Scientific** A11011	Donkey	1:1000

6. Results

6.1. Co-immunoprecipitation assay shows varying ability of the LRRK2 phosphomutants to interact with 14-3-3

To determine possible differences in LRRK2:14-3-3 interaction when testing specific treatments, a set of controls for this interaction must be prepared, using different phosphomutants in the LRR cluster. An effective way to test the ability of two proteins to form a complex is by co-immunoprecipitation. This technique is based on the use of specific antibodies to capture a desired protein and all its interactors. We designed a co-immunoprecipitation assay based on the use of anti-Flag M2 antibodies attached to magnetic beads, to capture Flag-tagged LRRK2 variants and their interactome. Flag-tagged LRRK2 variants, including phosphomutants 6xS>A and 6xS>D, were transfected in HEK293T cells alongside Myc-tagged 14-3-3ζ, and cell lysates were incubated with Flag-M2 beads. The resulting immunoprecipitate (IP) was then used in western blot to determine the presence of 14-3-3 in the interactome of the LRRK2 variant. To properly interpret such signal, a small quantity of full lysate was kept as a control, here called input, and both the input and the IP were blotted for LRRK2, the loading control α-tubulin, and Hsp90. Hsp90 is a known interactor of LRRK2 (Nichols *et al.*, 2010) and can be used as a positive control for the co-immunoprecipitation. The resulting CoIP showed a strong interaction between WT LRRK2 and 14-3-3ζ (*figure 9*), which was completely lost when either serine 910 or serine 935 were mutated to alanine (*figure 9*). Interaction with 14-3-3 was instead maintained when serines 955/973, two heterophosphosites of the LRR cluster, were mutated to alanine. As expected, the phosphodead mutant 6xS>A is not able to interact with LRRK2, but unexpectedly, this was also true for the phosphomimetic 6xS>D mutant, suggesting that the negative side groups of aspartate fail to mimic a phosphate group (*figure 9*). The loading control α-tubulin was not homogeneous among the input blot, but the possibility of an unbalanced loading is excluded, as signal for Hsp90, which is also a housekeeping gene (*figure 9*), is homogeneous among input samples. This also suggests that for future Co-IPs α-tubulin could be entirely omitted in favour of using Hsp90 as a control for both gel loading and immunoprecipitation.

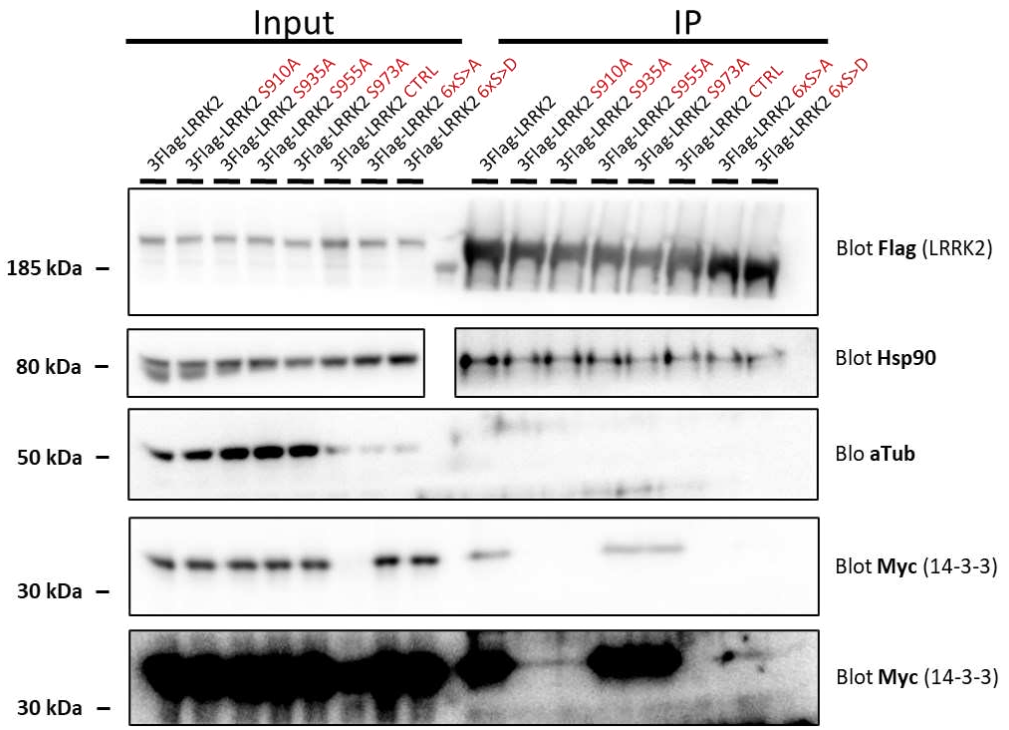

Figure 9 - LRRK2 phosphomutants Co-immunoprecipitation analysis *of the interaction between different 3xFlag tagged LRRK2 phosphomutants and 14-3-3ζ. HEK293T were co-transfected with a different LRRK2 phosphomutant, noted in red, and Myc-14-3-3ζ. Two control conditions were included, one with cotransfection of LRRK2 WT and Myc-14-3-3, the other with transfection of only LRRK2 WT, identified in red as LRRK2 CTRL. On the left, the western blot of whole cell lysates is presented (Input), with blots for Flag, Hsp90, α-tubulin and Myc. On the right, the western blots of the immunoprecipitated proteins obtained by Co-immunoprecipitation with anti-Flag M2 magnetic beads. The blot for Myc (14-3-3) is presented with two different contrast adjustments to show proteins present in a low quantity.*

6.2. MLi-2 dose range assay for pS935 LRRK2 levels

6.2.1. Dotblot assay and western blot assay results on pS935 ratio do not differ significantly

MLi-2, like other type I LRRK2 kinase inhibitors, induces in cell culture the dephosphorylation of serine 935 LRRK2 in a dose dependent manner and this can be used as a readout of LRRK2 sensitivity to MLi-2. To determine differences in sensitivity of LRRK2 to the inhibitor, a dose-response curve was prepared by measuring the levels of pS935 LRRK2 when cells were treated with increasing concentrations of MLi-2. To do this, one can perform a classical western blot, with gel electrophoresis to separate proteins of different size. This allows for minimum undesired background, but requires time and the use of a gel, which normally has limited space for samples. Moreover, when proteins are divided by size, the protein of interest needs to be present in a single, clear band, representing its complete form. Another option is to use a scalable, dotblot assay, described in more detail in the materials and methods section. This low-tech and low-cost technique allows for the fast analysis of many samples, at the cost of size differentiation since all the proteins coming from the lysates are concentrated in the same point. Considering

that our study of the effects of MLi-2 at different concentrations requires a high number of samples for each replicate, we investigated whether the dotblot assay would be a viable alternative to western blot. Dose-response curves of the same samples, obtained with dotblot and western blot, were compared (*figure 10*). Cells co-expressing 3xFlag-LRRK2 WT and 14-3-3ζ or difopein were treated for 1 hour with MLi-2, going from 0.3 nM to 1000 nM. Although western blot presents a lower starting phosphorylation level, the IC50 obtained from the two assays does not vary significantly (p=0.6189). This is because the IC50, or half maximal inhibitory concentration, is a relative measure, indicating at which concentration the dose-response curve is halfway between the plateaus at the ends.

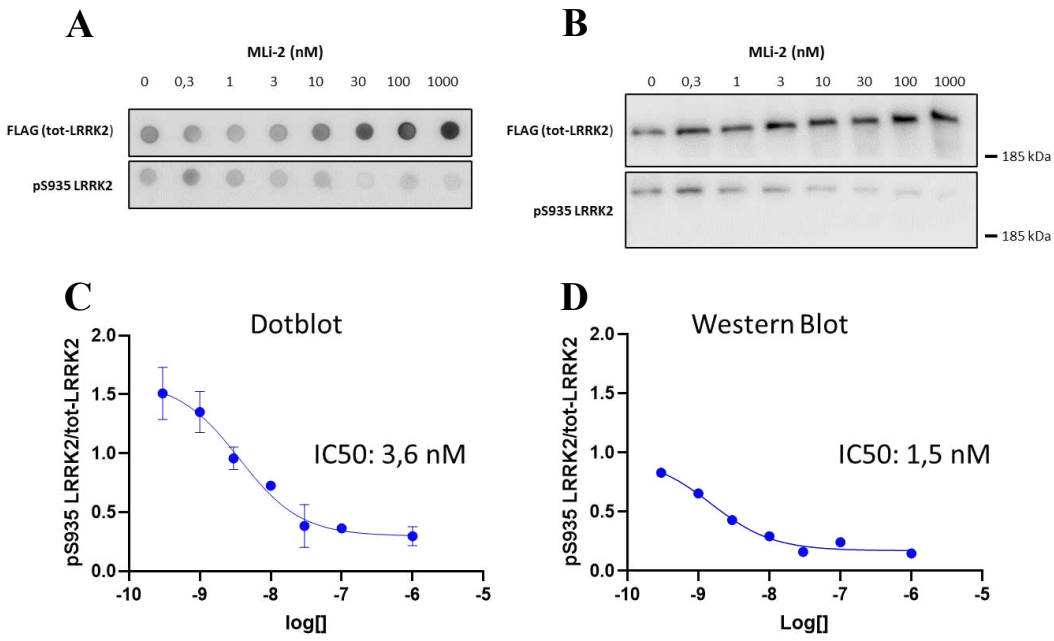

Figure 10 - determination of viability of the dotblot assay

*Dotblots and western blot were performed on HEK293T cells co-transfected with 3xFlag-LRRK2 WT + empty backbone (CMV), after treatment for 1 h with MLi-2 at different concentrations. (**A**) Exemplary blot of the dotblot assay, incubated with either anti-FLAG antibody or anti-pS935 LRRK2 antibody, showing a clear progressive reduction in phosphorylation. (**B**) Western blot performed on the same samples. (**C**) ratio pS935/tot-LRRK2 coming from the dotblot assay and (**D**) the same analysis performed using data coming from the western blot assay (N=1). Comparison of IC50 values was performed with extra sum-of-squares F test (p-value threshold p=0.05).*

6.2.2. Difopein expression incudes an important dephosphorylation of LRRK2

Studies have shown that 14-3-3 overexpression can increase phosphorylation levels on this serine, while difopein has an opposite effect (Lavalley *et al.*, 2016). Knowing this, we tried to determine whether difopein expression/14-3-3ζ overexpression could affect the ability of MLi-2 treatment to induce S935 dephosphorylation. Our hypothesis was that kinase inhibition by MLi-2 alters the mechanism responsible for phosphorylation of the heterophosphosites, which would then be dephosphorylated by phosphatases like PP2. In this hypothesized mechanism, 14-3-3 acts as a shield for the heterophosphosites, so the protein's overexpression would temporarily prevent dephosphorylation by shielding the

serines. This would translate into a shift in the dose-dependent curve describing the ratio of LRRK2 with phosphorylated serine 935 (pS935) over the total LRRK2. More specifically, the shift induced by 14-3-3 overexpression would induce an increase in the IC50; on the contrary, difopein expression should accelerate the dephosphorylation, because 14-3-3 would be unable to interact with LRRK2. Thus, effects of 14-3-3/difopein can be determined by analysing differences in IC50 with the control.

Having determined the dotblot assay to be a viable alternative to western blot, we moved on to prepare dotblot assays for a control, expressing LRRK2 WT and empty vector (CMV), a condition with overexpression of 14-3-3ζ, and another condition with expression of difopein. For each condition, 8 independent samples were prepared to be treated with increasing concentrations of MLi-2. One sample for each condition was left without treatment, to analyse the effects of 14-3-3/difopein expression, and to normalize the data of the following dose-response curves. When compared to the CMV control treated with DMSO, difopein expression caused a strong reduction in pS935 LRRK2 (p=0.0042), but 14-3-3 overexpression did not induce a significant increase in phosphorylation of LRRK2 (p=0.5124), possibly suggesting that S935 phosphorylation is close to saturation (*figure 10*).

6.2.3. 14-3-3 overexpression does not affect dose-response curve of MLi-2 induced pS935 LRRK2 dephosphorylation, while difopein expression induces dephosphorylation independently from the effect of MLi-2

After the effect of the simple expression of 14-3-3/difopein was determined, we moved on to determine IC50 shifts using the dose-response curves. The most striking difference was a significant decrease in LRRK2 phosphorylation when difopein was introduced (*figure 11*). A dose-response curve was still maintained, meaning that both difopein and MLi-2 affected LRRK2 phosphorylation, and the IC50 did not significantly differ from the CMV control (p=0.3921). On the other hand, samples overexpressing 14-3-3ζ were not significantly different in any way from the control CMV (*figure 11*).

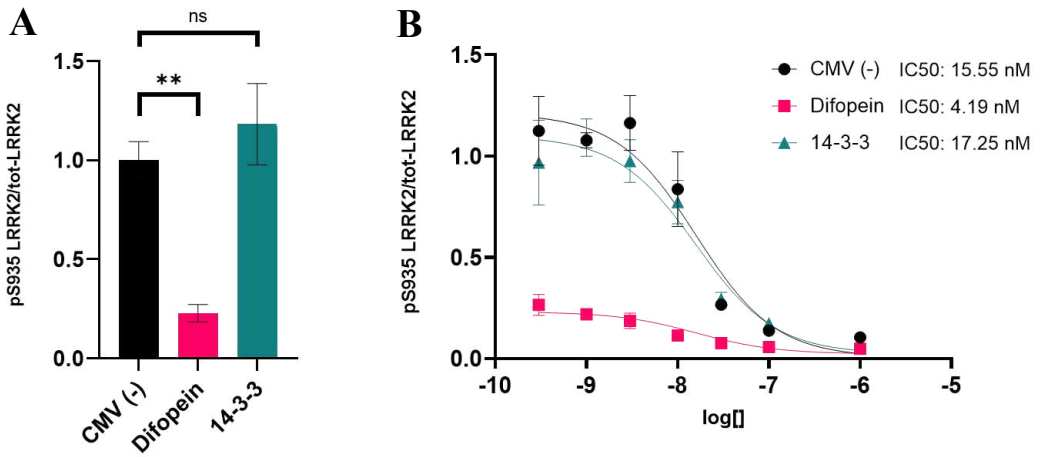

Figure 11 - MLi2 Dose range

*(**A**) Ratio of pS935 LRRK2 over LRRK2 was determined via dotblot. HEK293T cells were co-transfected with 3xFlag tagged LRRK2 WT and either eYFP-difopein or Myc-14-3-3. The negative control CMV presents co-transfection of 3xFlag-LRRK2 and empty vector. Ratios were normalized over the negative control CMV. Statistical analysis was performed via ordinary one-way ANOVA. The experiment was performed in 4 replicates (N=4). (**B**) Ratio of pS935 LRRK2 over total LRRK2 was determined via dotblot and plotted against the concentration of MLi2 used for treatment, ranging from 0.1 nM to 1000 nM. HEK293T cells were co-transfected with 3xFlag tagged LRRK2 WT and either eYFP-difopein or Myc-14-3-3. The negative control CMV presents co-transfection of 3xFlag-LRRK2 and empty vector. Ratio values were normalized over the CMV sample treated with DMSO. Comparison of IC50 values was performed with extra sum-of-squares F test (p-value threshold p=0.05). No significant difference in IC50 was detectable (p=0.6978). All data is presented as mean + SEM. The experiment was performed in 4 replicates (N=4).*

6.3. Immunocytochemistry assay to study LRRK2 subcellular localization phenotypes

It is known that 14-3-3 modulates the subcellular localization of LRRK2, maintaining LRRK2 diffusedly distributed in the cytosol, and that disruption of the interaction via phosphodead mutants causes the accumulation of LRRK2 in discrete cytoplasmic pools (Nichols *et al.*, 2010). It is also known that MLi-2 treatment causes LRRK2 to associate to microtubules in an orderly manner, creating filamentous structures (Marchand *et al.*, 2022). Knowing this, we decided to investigate the possible subcellular localization phenotypes associated with different conditions. Such an analysis could lead to the identification of conditions with specific phenotypes, different from wildtype, useful in determining the effectiveness of various PD treatments on LRRK2. Three different LRRK2 variants, WT, 6xS>A and 6xS>D, were transfected in HEK293T cells. For each protein variant, six conditions were prepared: control expressing empty plasmid, 14-3-3ζ, difopein expression, mutant R18 expression (called here difopein CTRL) as a control for difopein, CMV expression + MLi-2 treatment, 14-3-3ζ overexpression + MLi-2 treatment. Cells were subjected to immunocytochemistry (*figure 12*) to visualize at the microscope both the correct cotransfection of the desired plasmids and the LRRK2 subcellular localization phenotype.

Four different phenotypes of LRRK2 subcellular localization were previously described (Drouyer *et al.*, 2021). These include cytoplasmic diffusedly distributed LRRK2 (called here cytosolic), filamentous structures (called here filaments), small punctate accumulations (called here punctate) and larger amorphous accumulation

(*figure 13*). For each of the 18 total conditions, cell counting was performed manually, assigning to all the properly cotransfected healthy cells a single phenotype out of the four, creating in the end a proportion of the presence of each phenotype in each condition.

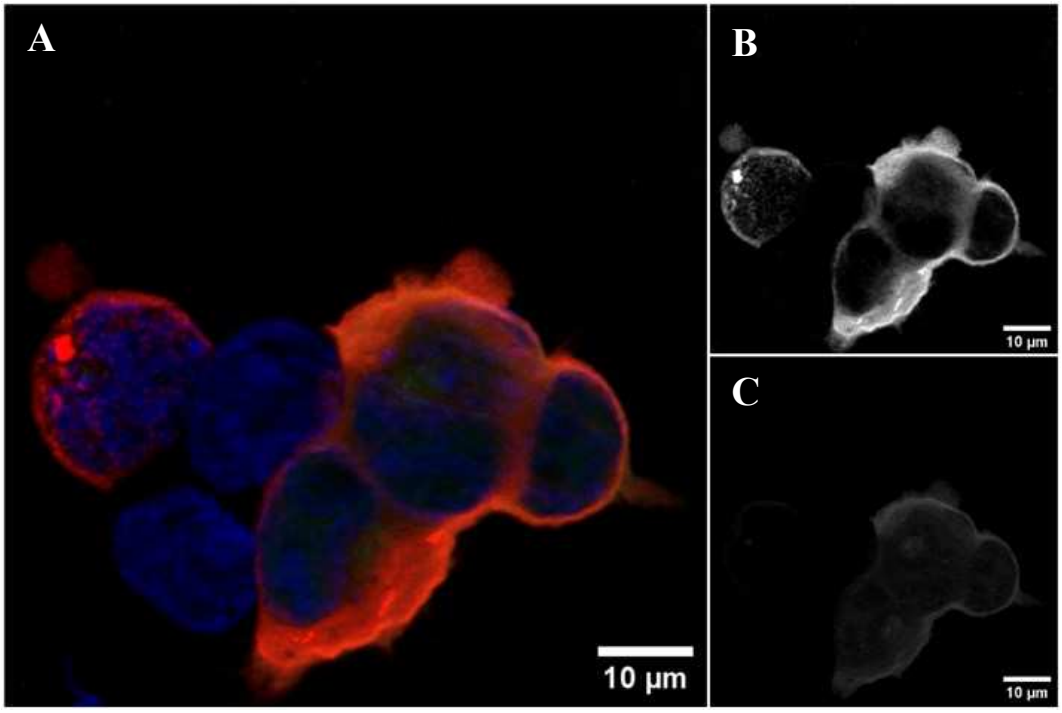

Figure 12 - Representative result of immunocytochemistry assay

*A representative picture of the immunocytochemistry results is presented, to show how successful co-transfection of both LRRK2 and 14-3-3/difopein/difopein CTRL is identified. (**A**) Cells transfected with 3xFlag-LRRK2 WT and eYFP-Difopein CTRL are shown as the merge of all channels used to visualize the cells. Cells were incubated with primary antibodies rabbit anti-LRRK2 and mouse anti-Myc (to target 2xMyc-14-3-3). Incubation was then performed with secondary antibodies conjugated with Alexa Fluor dies anti-mouse Alexa Fluor 488 (green) and anti-rabbit Alexa Fluor 568 (red). Cells were finally stained with DAPI (blue) for nuclei identification. No antibody was necessary against difopein or difopein CTRL, because of the eYFP-tag. Co-transfection is visible as orange because of the mixing of red and green signal (**B**) Red channel, identifying LRRK2 in the transfected cells. (**C**) Green channel, identifying difopein CTRL. The signal levels coming from anti-mouse Alexa Fluor 488 for 14-3-3 and from the eYFP tag on difopein and difopein CTRL were of comparably high strength.*

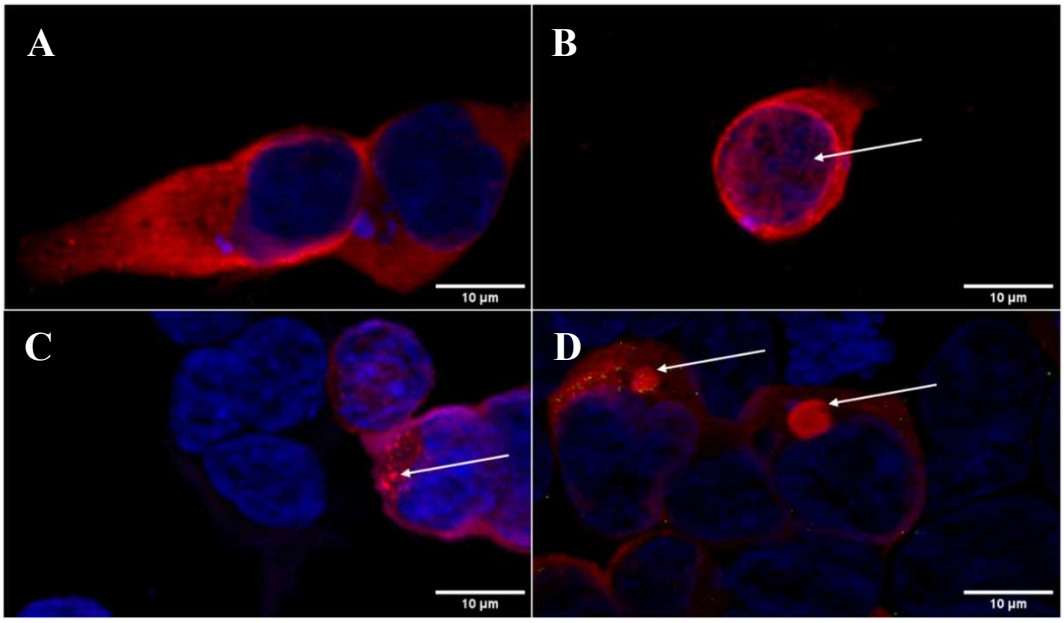

Figure 13 - LRRK2 subcellular localization phenotypes

*Cells that showed proper co-transfection by the emission of light for both red and green filters were manually identified and counted as one of 4 LRRK2 subcellular localization phenotypes. (**A**) Cytosolic phenotype. In WT conditions, LRRK2 is diffused in the cytosol, creating an even signal outside of the nucleus that we define as "cytosolic". (**B**) Filaments phenotype. When kinase activity is inhibited with MLi-2, LRRK2 proteins associate with microtubules, creating filamentous structures throughout the cell. These filaments are variable in length and do not present a repeating organization between cells. (**C**) Punctate phenotype. Studies have previously shown that the LRRK2 phosphomutant 6xS>A, unable to create the LRRK2:14-3-3 complex, condenses into cytosolic pools that we define as "punctate". Such punctate do not have regular shapes and can appear more or less circular. (**D**) Amorphous accumulation phenotype. Another documented subcellular localization phenotype of LRRK2 is an accumulation of the protein is a single point of the cytosol, creating a well-defined large spot that we label as "amorphous accumulation".*

6.3.1. 14-3-3 overexpression has no effect on the MLi-2 dependent microtubule association of LRRK2

After calculating the proportions of each subcellular localization phenotype for the studied phenotypes, we investigated what are the possible differences of the condition with the corresponding control. The conditions studied included, for each of the three LRRK2 variants (LRRK2 WT, phosphomutant LRRK2 6xS>A or phosphomimetic LRRK2 6xS>D): control condition with empty backbone transfected (**CMV**); 14-3-3ζ overexpression (**14-3-3**); difopein expression (**difopein**); mutant R18 peptide (**difopein CTRL**); MLi-2 kinase inhibitor treatment + empty backbone (**Mli-2**); MLi-2 kinase inhibitor treatment + 14-3-3ζ overexpression (**14-3-3 + MLi-2**). This experiment is performed as a pilot experiment to identify specific conditions in which 14-3-3 affects LRRK2 subcellular distribution that may be the focus of follow up studies. We started by analysing all the different conditions with a shared LRRK2 variant.

First, we found that in LRRK2 WT samples, overexpression of 14-3-3ζ does not induce any significant variation in the proportion of different localization phenotypes when compared to the control, with the vast majority of observed cells presenting a diffuse cytosolic LRRK2 (*figure 14*). Difopein expression caused an important decrease in cytosolic LRRK2 (p= =0.0218) and a trend to increase

punctate formation (p=0.0663), while not significantly affecting filaments formation (p=0.0925). This was not seen when difopein CTRL was introduced, proving that the variation in the difopein condition is caused by the disruption of 14-3-3 binding (*figure 14*). As previously shown in the literature, MLi-2 treatment caused a significant increase in the proportion of cells with filaments (p=0.0037). Importantly, this was true also when alongside kinase inhibitor treatment 14-3-3 was overexpressed (p=0.0093), indicating that 14-3-3 is not able to counteract the effect of MLi-2 on LRRK2 subcellular localization.

When comparing LRRK2 6xS>A conditions with the corresponding control, no significant difference in any of the 4 phenotypes was noted for 14-3-3, difopein or difopein CTRL conditions. This is likely caused by the inability of the phosphodead LRRK2 mutant to interact with 14-3-3, making LRRK2 6xS>A unaffected by neither the 14-3-3 protein itself nor the inhibitor of 14-3-3 protein-protein interactions. Similarly to what was seen with LRRK2 WT, MLi-2 treatment caused an increase in cell presenting filaments (p=0.0217), with a significant decrease in cells presenting punctate (p=0.0178). This was however not seen when MLi-2 treatment was paired with 14-3-3 overexpression (p=0.1081). The same condition also a significant increase in the amorphous accumulation proportion (p=0.0354).

Conditions with cells expressing LRRK2 6xS>D had similar results to LRRK2 WT for 14-3-3 overexpression and difopein CTRL expression, with no significant variation from the control. However, unlike LRRK2 WT, this was also the case for difopein expression, meaning that inhibition of LRRK2 6xS>D:14-3-3 interaction did not affect the subcellular localization of LRRK2. MLi-2 treatment was still effective in stimulating filaments formation, both when treatment was isolated (p=0.0059) and when accompanied by 14-3-3 overexpression (p=0.0037). Additionally, simple MLi-2 treatment caused a reduction in the proportions of cells presenting punctate, rather than affecting the proportion of cytosolic LRRK2 (p=0.0323).

6.3.2. Phosphomutant LRRK2 variants significantly differ from LRRK2 WT in their subcellular localization phenotypes, except when cells are treated with MLi-2

Using the same data for the previous analysis, we then moved on to determine any differences in proportions of LRRK2 subcellular localizations when the LRRK2 phosphomutants are compared to the control LRRK2 WT for the same condition, to isolate the effect of the mutations on the LRRK2 protein.

Both 6xS>A and 6xS>D varied significantly from the control, with LRRK2 6xS>A presenting a decrease in cytosolic LRRK2 (p=0.0253) and a trend to an increase proportion of cells presenting punctate (p=0.0736), while 6xS>D had a significant increase in the punctate proportion (p=0.0253). Similar results were seen when 14-3-3 was overexpressed, with a trend in a higher proportion of punctate for 6xS>A (p=0.0526). LRRK2 6xS>D showed both a significantly higher proportion of punctate (p=0.0396) and a smaller proportion of cytosolic LRRK2 (p=0.0171).

Intriguingly, LRRK2 WT and LRRK2 6xS>A present similar proportion for all phenotypes.

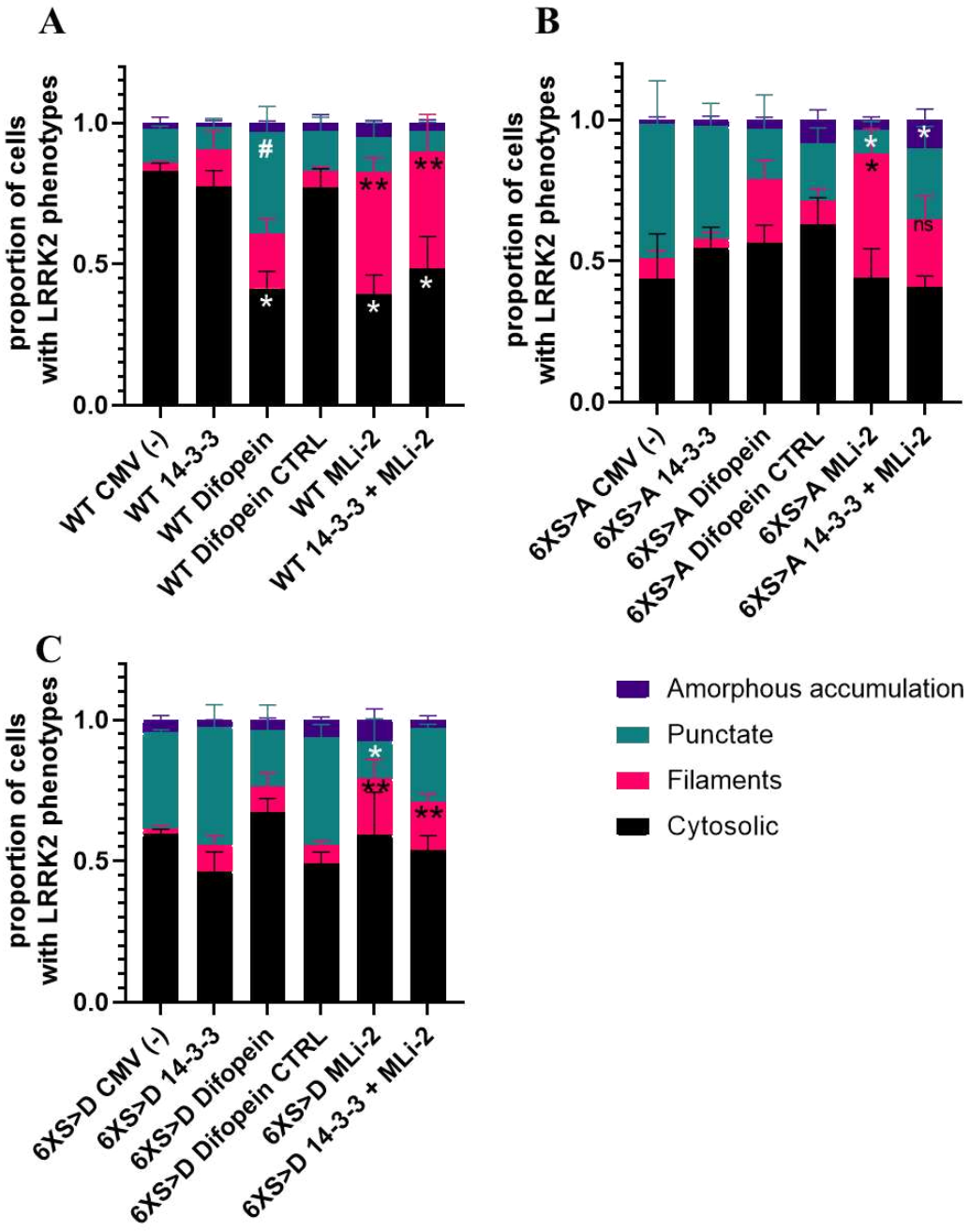

Figure 14 - Proportions of LRRK2 subcellular localization phenotypes within the same LRRK2 variant
*The comparisons between different test conditions when using the same LRRK2 variant are here shown. The conditions tested are, in order: control (**CMV**); 14-3-3ζ overexpression (**14-3-3**); difopein expression (**difopein**); mutant R18 peptide expression (**difopein CTRL**); MLi-2 treatment at 10 nM for 1 hour (**MLi-2**); MLi-2 treatment at 10 nM for 1 hour, alongside 14-3-3 overexpression ζ (**14-3-3** + **MLi-2**). Proportions of cellular phenotypes between samples expressing LRRK2 WT (**A**), LRRK2 6xS>A (**B**) and LRRK2 6xS>D (**C**) are shown. Statistical analysis was performed via uncorrected Kruskal Wallis test (p-value threshold p=0.05). Counting was performed on 3 independent replicates (N=3).*

The only variation was for an increase in LRRK2 6xS>D cytosolic proportion (p=0.0253). Samples expressing difopein CTRL and LRRK2 6xS>A again showed no difference with the corresponding control, while cells expressing LRRK2 6xS>D presented a higher proportion of punctate (p=0.0253) and a smaller proportion of cytosolic diffuse LRRK2 (p=0.0369). Finally, the response of cells expressing any of the LRRK2 variants to the MLi-2 treatment did not vary significantly in any of the proportions, no matter whether treatment was isolated or alongside 14-3-3 overexpression (*figure 15*).

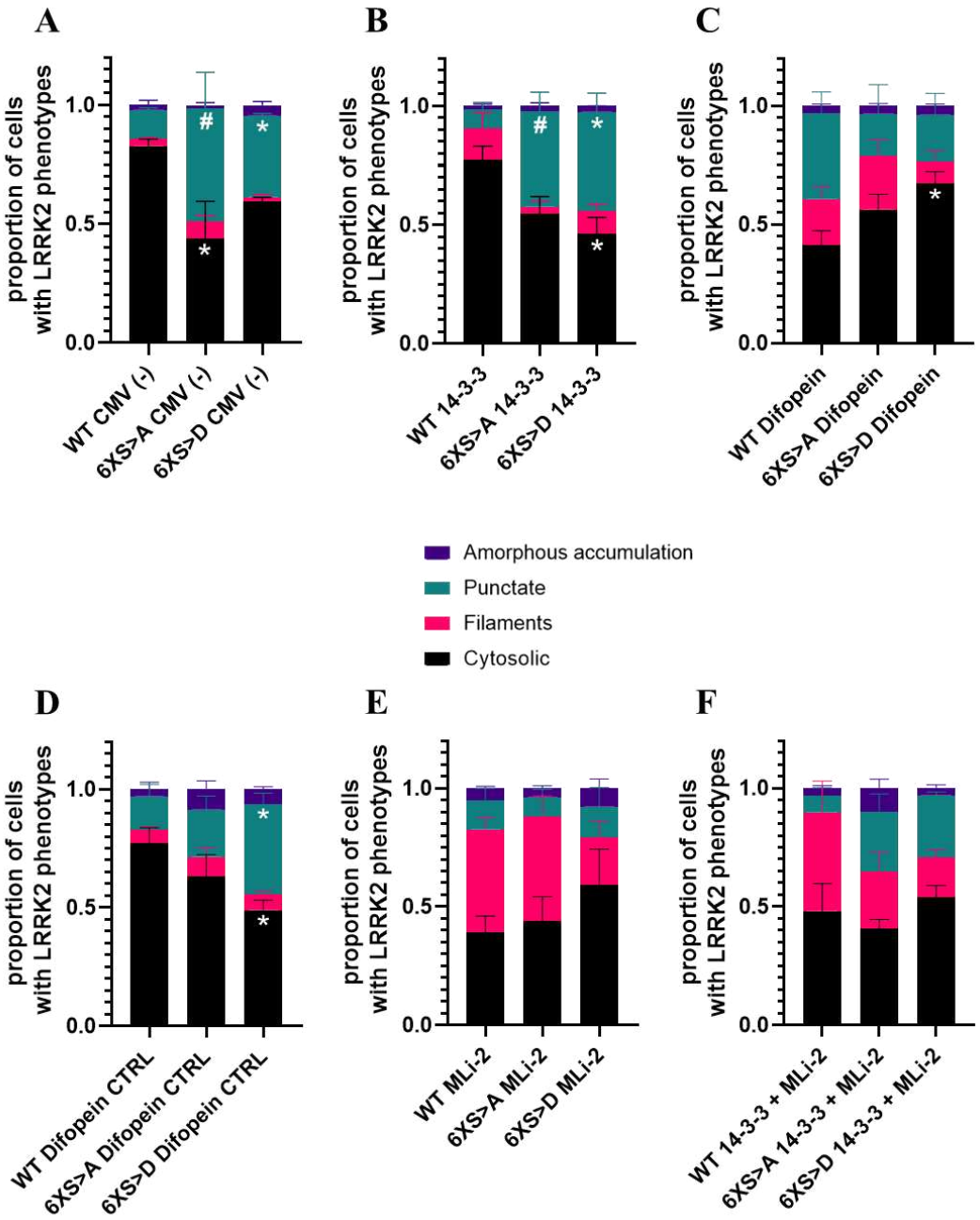

*Figure 15 - **Proportions of LRRK2 subcellular localization phenotypes between different LRRK2 variants***
*The comparisons between the same test conditions when using different LRRK2 variants are shown, in order to determine the presence of phenotype differences of LRRK2 phosphomutants in respect to the WT control. The condition presented are as follows: (**A**) control (**CMV**); (**B**) 14-3-3ζ overexpression (**14-3-3**); (**C**) difopein expression (**difopein**); (**D**) mutant R18 peptide expression (**difopein CTRL**); (**E**) MLi-2 treatment at 10 nM for 1 hour (**MLi-2**); (**F**) MLi-2 treatment at 10 nM for 1 hour, alongside 14-3-3 overexpression ζ (**14-3-3 + MLi-2**). Statistical analysis was performed via uncorrected Kruskal Wallis test (p-value threshold p=0.05). All measurements were performed on 3 independent replicates (N=3).*

7. Discussion

In this work, we have studied the molecular and cellular phenotypes associated with the LRRK2:14-3-3 complex via the use of different techniques and under various conditions affecting the interaction between the two proteins. The ability of LRRK2 variants to form complexes with 14-3-3 was determined by co-immunoprecipitation, with the aim of identifying potential controls for the LRRK2:14-3-3 interaction. The possible interplay between 14-3-3 and the type I kinase inhibitor for LRRK2 MLi-2 was studied by determining changes in the phosphorylation of LRRK2. The subcellular localization of LRRK2 was then observed, to explore how conditions altering formation of LRRK2:14-3-3 can influence this phenotype. Here, we present an analysis and interpretation of our data, taking into account the existing literature on LRRK2 and 14-3-3.

7.1. Co-immunoprecipitation

The co-immunoprecipitation assay is a useful technique for determining the ability of two proteins to form complexes together. Our results show how the mutation of known heterophosphosites in the LRR cluster affects LRRK2's ability to interact with 14-3-3 and form a complex. More specifically, interaction is impaired when either one of the serines 910 and 935 are mutated into alanine, while this effect is not seen for the LRRK2 S955A/S973A. This confirms that phosphorylation on S910 and S935 are both needed for the interaction and confirms these phosphomutants as negative controls. Similar levels of 14-3-3 in the affinity purified complexes were seen also for the phosphodead mutant LRRK2 6xS>A. Considering that there is no appreciable difference for LRRK2:14-3-3 interaction between LRRK2 S910A, LRRK2 S935A and LRRK2 6xS>A, the latter could suffice as a general negative control. Interestingly, when increasing contrast on the blot for immunoprecipitated 14-3-3, the same phosphodead LRRK2 mutants still showed a very weak signal for the protein. This signal was stronger than the background detection signal of the Myc tag primary antibody, as shown in the negative control with transfection of the single LRRK2 WT plasmid and no overexpression of 14-3-3 (*figure 9*). The significance of this difference is not clear, as it could be simply due to the residual binding of 14-3-3 to the anti-Flag affinity beads, but the existence of a secondary, weaker interaction site between the two proteins is also a possibility. This secondary binding site would be in any case weaker than the one on the LRR cluster. Further research is required to elucidate this possibility.

Unexpectedly, the phosphomimetic mutant LRRK2 6xS>D lost the ability to interact with 14-3-3 as well. This indicates that aspartic acid does not chemically resemble phosphorylated serine enough and the mutation of the serines possibly induces a change in the local secondary structure of LRRK2 from the WT. Thus, our results do not support the use of LRRK2 6xS>D as a positive control for the interaction. Aside from aspartic acid, another amino acid commonly used to mimic phosphorylation is glutamic acid. Considering the importance of a viable positive

control for LRRK2:14-3-3 interaction, testing a LRRK2 6xS>E phosphomimetic mutant should be considered for the future. It is also possible the hypothesized conformational change in LRRK2 caused by the mutation of 6 heterophosphosites does not occur when single serines are mutated. Thus, the effect of LRRK2 S910D and LRRK2 S935D on the ability to form complexes with 14-3-3 needs to be tested.

Furthermore, analysis of the LRRK2:14-3-3 interaction must be explored by other techniques, such as proximity-dependent biotin identification (BioID), a technique that allows to selectively tag and isolate the interactors of a protein of interest in living cells. A modified version of the *Escherichia coli* protein ligase BirA is fused to the protein of interest. The modified BirA, called BioID, can perform a promiscuous biotin ligase activity, therefore biotinylating surrounding proteins (Sears *et al*., 2020) in a proximity dependent manner. Therefore, biotin-tagged proteins can be assumed as interactors of the protein of interest. As such, when providing to live cells biotin, BioID will tag the interactors of the protein of interest, which can then be isolated via the use of streptavidin beads, and later identified via western blotting or mass spectrometry. An important advantage of BioID is that it is better suited to identify transient interaction that occur in live cells as parts of specific pathways.

7.2. MLi-2 dose range and its effect on LRRK2 S935 phosphorylation

Here, we validate the dotblot protocol quantitatively detecting total and S935 phosphorylated LRRK2 as a cost-effective, high throughput and low-tech option for testing IC50 measurements for compounds that affect LRRK2 S935 phosphorylation.

When isolating the effect of expression of 14-3-3ζ or difopein, on the pS935-LRRK2 signal, in basal conditions (i.e. without MLi-2 inhibitor), difopein had a strong effect on the phosphorylation of LRRK2, reducing it significantly when compared to the control. This aligns with the hypothesized role of 14-3-3 in maintaining phosphorylation of the LRR cluster by shielding it from the effect of phosphatases and validates difopein as an effective inhibitor of the LRRK2:14-3-3 interaction. By contrast, 14-3-3 overexpression did not significantly increase S935 phosphorylation when compared to the control.

The dose response curve to MLi-2 were then compared to determine whether 14-3-3 or difopein could affect LRRK2's sensitivity to the inhibitor for the LRRK2 S935 phosphorylation rates. When compared to the control, the dose-response curves of 14-3-3ζ or difopein expressing cells showed no significant effect on IC50. In particular, difopein caused an overall strong reduction of pS935 levels, but this effect was independent of MLi-2 concentration, since a dose-dependent decrease of phosphorylation was also present. Our hypothesis that difopein expression would increase sensitivity LRRK2 S935 phosphorylation to MLi-2, shifting the dose-response curve to lower concentrations of the inhibitor, is not supported by our

results. Likewise, 14-3-3 overexpression does not significantly protect against inhibitor induced dephosphorylation on S935, under the conditions tested. Considering that type I kinase inhibitors are known to cause conformation shifts in the LRRK2 protein, a possible explanation of this is that MLi-2 treatment modifies the 14-3-3 binding site on LRRK2, thus blocking the interaction and exposing the heterophosphosites to phosphatases. Since difopein acts on the 14-3-3 protein to block interaction with all its targets, difopein's effect on LRRK2 phosphorylation is independent from MLi-2 treatment. However, MLi-2 itself renders LRRK2 unable to interact with 14-3-3, so difopein has no effect on this. These results suggest that type I kinase inhibitors induce dephosphorylation of serine 935 by inducing a conformational shift that disrupts the LRRK2:14-3-3 interface. It is known that type I inhibitors bind LRRK2 in its closed active conformation, rendering the LRRK2 kinase unable to accept ATP in its ATP-binding pocket (Tasegian *et al.*, 2021). Considering that 14-3-3 keeps LRRK2 in less active and monomeric form, a possible explanation is that the affinity to 14-3-3 of LRRK2 is decreased when going from the closed inactive state to the active one. However, this possibility needs to be further explored, for example by using different isoforms of 14-3-3, like 14-3-3γ. As such, even if our results have not shown any change in MLi-2 sensitivity, the potential efficacy in the study of the LRRK2:14-3-3 interaction of type I inhibitors dose-response curves for the phosphorylation of serine 935 is still unclear. The next logical step in research consists in the use of type II kinase inhibitors, which keep LRRK2 in an open, inactive form. Preliminary research has found that some type II kinase inhibitors for LRRK2 do not induce a dephosphorylation of S935, while still affecting markers of LRRK2 activity, like phosphorylation of its targets (Tasegian *et al.*, 2021). While the type II kinase inhibitors tested are still imperfect in terms of efficacy and specificity, they may be conceptually of significant interest, as the ability to block LRRK2's kinase activity while keeping the protein in its inactive form could provide a useful positive control for kinase activity. Moreover, their interaction with 14-3-3 remains to be explored.

7.3. LRRK2 subcellular localization and its 14-3-3 dependency

In this pilot experiment, we wanted to identify possible modifications in the LRRK2 subcellular localization in different conditions that alter LRRK2:14-3-3 interaction.

First, our immunocytochemistry data shows a trend in cells expressing LRRK2 WT and difopein to form a punctate phenotype, similarly to what was previously seen for the phosphodead mutants S910A and S935A (Doggett *et al.*, 2012). This is interesting, as punctate formation could potentially become a marker of the loss of LRRK2:14-3-3 interaction. Moreover, previous research had reported that difopein de-stabilized cytosolic LRRK2, but in a similar way to kinase inhibitor treatment, with microtubule association (Zhao *et al.*, 2015). Further investigation of the differences between difopein and kinase inhibitor is needed, especially considering

that it is not clear how destabilization of cytosolic LRRK2 with punctate formation affects LRRK2 activity.

Cells overexpressing LRRK2 WT presented as expected a diffused cytosolic phenotype, with a low proportion of cells with punctate, filaments or amorphous accumulation. By contrast, the simple overexpression of the phosphomutant LRRK2 6xS>A, when compared to LRRK2 WT, showed an important increase in the cells presenting a punctate phenotype and no change in its LRRK2 subcellular localization phenotypes when either 14-3-3, difopein or difopein CTRL were expressed. This is in line with what was expected, as the phosphodead mutations on the LRRK2:14-3-3 interaction site render LRRK2 unable to respond to neither 14-3-3 overexpression nor 14-3-3 inhibitors. This again confirms the viability of LRRK2 6xS>A as a negative control of the interaction.

Interpretation of the results for phosphomimetic mutant LRRK2 6xS>D is challenging when observed alone but becomes clearer once the result of the other experiments are taken into account. Nowadays, 14-3-3 is considered to be responsible for maintaining LRRK2 in the cytosol. If mutation of serine to aspartic acid was effective in mimicking phosphorylation on serine, it would be expected to see no difference in phenotype proportions between the control CMV and 14-3-3ζ overexpression. This was indeed the case for LRRK2 6xS>D CMV and 14-3-3 samples. However, difopein expression should then affect the proportion of cytosolic LRRK2, since difopein inhibits 14-3-3 to interact with any of its targets. Instead, samples expressing difopein did not differ from the control. This result is in line with the loss of 14-3-3 interaction reported in the co-immunoprecipitation analysis. This was also reflected in the comparison between LRRK2 variants for each condition, where LRRK2 6xS>D significantly differed from WT for the 14-3-3, difopein and difopein CTRL samples (*figure 15*).

Importantly, MLi-2 was shown to induce the accumulation of LRRK2 to filamentous structures with all LRRK2 variants. 14-3-3 overexpression alongside treatment did not recover a cytosolic phenotype, aside from the LRRK2 6xS>A mutant where the non-significant difference could be due to high variability between replicates. All three tested LRRK2 variants also did not differ between each other for filaments proportion, with or without 14-3-3 overexpression. 14-3-3's inability to affect this phenotype correlates with what was shown in the dose range experiment, where 14-3-3 is unable to protect from MLi-2-associated LRRK2 dephosphorylation. The comparison between LRRK2 variants then leads to the conclusion that MLi-2 induces microtubule association with a mechanism that is somewhat disconnected from the phosphorylation state of the LRR cluster. It is unclear what is the physiological relevance of microtubule association. What is known is that some PD-associated LRRK2 mutants, like LRRK2 I2020T, present microtubule association, and recent studies have modelled the organization that LRRK2 takes when associating with microtubules (Watanabe *et al.*, 2020). Both LRRK2 I2020T and LRRK2 WT treated with MLi-2 were observed forming a right-handed double helix around the microtubules (Watanabe *et al.*, 2020). Importantly, oligomerization depends on both a WD40:WD40 interaction and a COR:COR

interaction, as some mutants for both domain are unable to associate to microtubules. This is interesting, because the dependency of association only on non-enzymatic LRRK2 domains towards the C terminus matches with our finding that changes to the non-enzymatic LRRK2 domains at the N terminus have no effect on microtubule association. In this new model, the KIN domain faces the cytosol, where it can potentially phosphorylate its targets. This matches with the increased kinase activity reported in PD-associated LRRK2 mutant that associate to microtubules. These recent results suggest that LRRK2 microtubule association is an important phenotype in the context of PD, so further research is needed to understand how this structure affects LRRK2 and its activity. These experiments suggest that the two phenotypes of filaments and punctate formation are mediated by independent mechanisms. More specifically, filaments formation is caused by the effect of type I kinase inhibitors on the LRRK2 conformation, with an effect similar to some pathogenic LRRK2 variants that carry mutations in the enzymatic domains. Punctate formation, on the other hand, seems to depend on the loss of interaction between 14-3-3 and LRRK2, as seen in both the phosphodead mutant LRRK2 6xS>A and in LRRK2 WT when difopein is provided (*figure 14).*

7.4. Future perspectives

The work of this master thesis focused on the identification of phenotypes of the LRRK2:14-3-3 complex in various conditions and with different techniques. Some of these results, specifically the dose range analysis of phosphorylation and the immunocytochemistry assay, require further replicates to confirm significant differences among the studied conditions with a reasonable confidence level. For the dose-range analysis, the use of new markers of LRRK2 kinase activity, such as the phosphorylation at the autophosphosite serine 1292 and the phosphorylation of a LRRK2's target like the RAB proteins, would provide a new perspective on the interplay between kinase inhibitors and 14-3-3 binding to LRRK2. New conditions for the dose-range analysis and the immunocytochemistry assay, such as treatment with type II kinase inhibitors like Ponatinib, GZD-824 and Rebastinib, need to be explored.

As presented before, the current hypothesis is that the LRRK2:14-3-3 interaction has a beneficial effect in PD by preserving LRRK2 phosphorylation on the heterophosphosites of the LRR cluster. What is not yet understood, however, is whether this beneficial effect stems from the protection of phosphorylation on the LRR cluster mediated by 14-3-3, or rather that it comes from how 14-3-3 itself modulates LRRK2's activity and subcellular localization. In other words: is strengthening the bond helpful because LRRK2 phosphorylation is protected by 14-3-3, or because 14-3-3's modulation of LRRK2 is preserved? The experiments here presented do not validate either of the two options, so new tests need to be designed to explore both possibilities. For this, the development of an effective way to constitutively phosphorylate the LRRK2 heterophosphosites in the LRR cluster would be most helpful.

The LRRK2:14-3-3 complex is a promising potential therapeutical target, as suggested by the documented positive effect of 14-3-3 on cellular phenotypes typical of PD-associated LRRK2 mutants (Lavalley *et al.*, 2016) and the reduced phosphorylation of LRRK2 on S910/S935 in PD-associated LRRK2 mutants, which renders 14-3-3 unable to interact with LRRK2 (Marchand *et al.*, 2020). It is important to keep in mind that the analyses presented in this master these do not validate nor invalidate the LRRK2:14-3-3 complex as a therapeutic target. To this end, the exploration of the effect of 14-3-3 overexpression on the phosphorylation and subcellular localization of PD-associated LRRK2 mutant is an important step in research. Research should also move on to LRRK2 phenotypes of higher physiological significance. An example of this would be LRRK2's presence in extracellular vesicles. It is known that LRRK2 plays an important role in vesicle trafficking, both for endosomal and lysosomal pathways. An important step for both pathways is the multivesicular body (MVB), a vesicular structure that forms intraluminal vesicles, which contain themselves cytosolic proteins. MVBs can fuse with the cell membrane, releasing the intraluminal vesicles to the extracellular space as what are then called exosomes, a type extracellular vesicle (EV). Crucially, LRRK2 has been found in extracellular vesicles and it has been reported that 14-3-3 mediates the process. For instance, inhibition of 14-3-3 using difopein, as well as LRRK2 kinase inhibition, is reported to block the release of LRRK2 in exosomes (Fraser *et al.*, 2013). Moreover, EVs coming from patients carrying PD-associated LRRK2 mutants are enriched for LRRK2 phosphorylated at S1292 (Taymans *et al.*, 2023b). PD was also associated with a decreased LRRK2 phosphorylation at S910 and S935 in EVs (Taymans *et al.*, 2023b), and in animals, inhibition of LRRK2 with kinase inhibitors led to a reduction in EVs of the levels of phosphorylated RAB10, a target of LRRK2 (Taymans *et al*, 2023b). In the context of our research mediating LRRK2 and 14-3-3 interaction, the levels of LRRK2, its targets and the phosphorylation of both in EVs represents a promising readout for changes in LRRK2 activity, as it more faithfully reflects the physiological state of the cell than the LRRK2 subcellular localization.

8. Conclusions

In this work, we have determined the ability of various LRRK2 mutants for the heterophosphosites at the LRR cluster to form complexes with 14-3-3 and determined LRRK2 6xS>A to be a valid negative control, while LRRK2 6xS>D does not function as a positive control. We have also explored the effect of 14-3-3 and difopein in altering the sensitivity of LRRK2 to the type I kinase inhibitor MLi-2, using the phosphorylation of serine 935 as a readout of LRRK2 kinase activity. In this case, our results indicate that neither 14-3-3 overexpression or difopein expression modulate the effect of MLi-2 on LRRK2. With an immunohistochemistry assay, we have assessed the subcellular localization assay of LRRK2 variants in various conditions altering interaction with 14-3-3, and found that the decrease in LRRK2:14-3-3 interaction has a distinct, punctate phenotype,

while the type I kinase inhibitor MLi-2 affects LRRK2 localization in an independent manner, inducing the formation of filaments (*figure 16*).

The role of the LRRK2 protein in Parkinson's disease has been the subject of study for many years. Moreover, interaction between LRRK2 and the 14-3-3 protein, a well-studied antiapoptotic modulator protein, represents a promising potential therapeutic target. However, the phenotypes associated with the LRRK2:14-3-3 complex are not yet completely understood. By studying the modulation of the LRRK2:14-3-3 complex, we have provided an array of phenotypes on which the study of LRRK2 and 14-3-3 can be further explored, with the hope in the future to find effective therapeutical strategies to tackle Parkinson's disease.

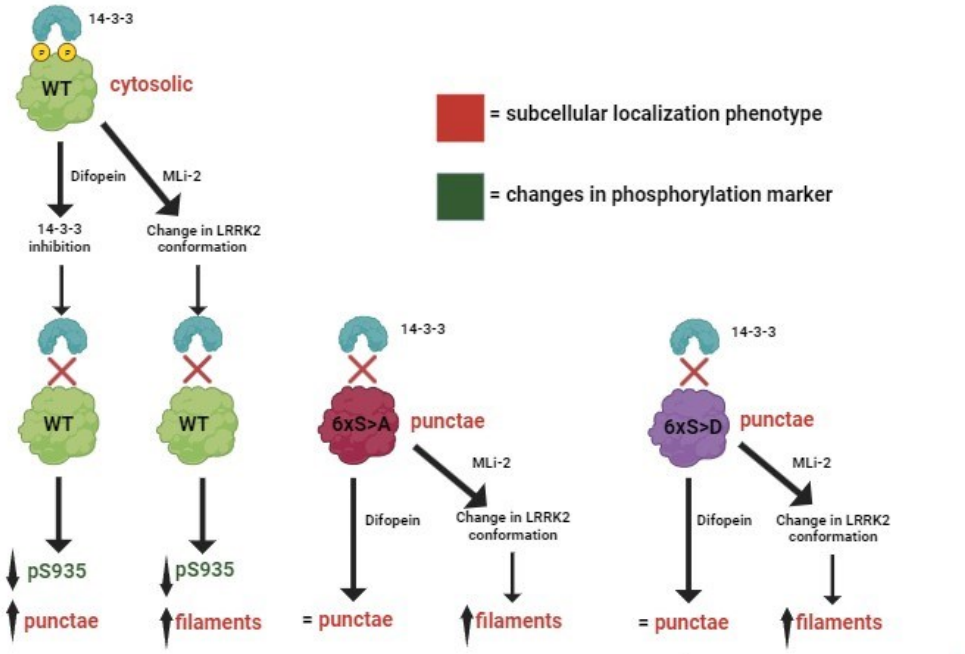

Figure 76 - Schematics of the results on LRRK2 subcellular localization and pS935 kinase activity marker

9. Bibliography

1. Wilson DM 3rd, Cookson MR, Van Den Bosch L, Zetterberg H, Holtzman DM, Dewachter I. Hallmarks of neurodegenerative diseases. *Cell*. 2023;186(4):693-714. doi:10.1016/j.cell.2022.12.032
2. Kalia LV, Lang AE. Parkinson's disease. *Lancet*. 2015;386(9996):896-912. doi:10.1016/S0140-6736(14)61393-3
3. Bendor JT, Logan TP, Edwards RH. The function of α-synuclein. *Neuron*. 2013;79(6):1044-1066. doi:10.1016/j.neuron.2013.09.004
4. Srinivasan E, Chandrasekhar G, Chandrasekar P, et al. Alpha-Synuclein Aggregation in Parkinson's Disease. *Front Med (Lausanne)*. 2021;8:736978. Published 2021 Oct 18. doi:10.3389/fmed.2021.736978
5. Luk KC, Lee VM. Modeling Lewy pathology propagation in Parkinson's disease. *Parkinsonism Relat Disord*. 2014;20 Suppl 1(0 1):S85-S87. doi:10.1016/S1353-8020(13)70022-1
6. Jankovic J, Tan EK. Parkinson's disease: etiopathogenesis and treatment. *J Neurol Neurosurg Psychiatry*. 2020;91(8):795-808. doi:10.1136/jnnp-2019-322338
7. Zhang X, Gao F, Wang D, et al. Tau Pathology in Parkinson's Disease. *Front Neurol*. 2018;9:809. Published 2018 Oct 2. doi:10.3389/fneur.2018.00809
8. Gan-Or Z, Liong C, Alcalay RN. GBA-Associated Parkinson's Disease and Other Synucleinopathies. *Curr Neurol Neurosci Rep*. 2018;18(8):44. Published 2018 Jun 8. doi:10.1007/s11910-018-0860-4
9. Myasnikov A, Zhu H, Hixson P, et al. Structural analysis of the full-length human LRRK2. *Cell*. 2021;184(13):3519-3527.e10. doi:10.1016/j.cell.2021.05.004
10. Soliman A, Cankara FN, Kortholt A. Allosteric inhibition of LRRK2, where are we now. *Biochem Soc Trans*. 2020;48(5):2185-2194. doi:10.1042/BST20200424
11. Berger Z, Smith KA, Lavoie MJ. Membrane localization of LRRK2 is associated with increased formation of the highly active LRRK2 dimer and changes in its phosphorylation. *Biochemistry*. 2010;49(26):5511-5523. doi:10.1021/bi100157u
12. Nichols RJ, Dzamko N, Morrice NA, et al. 14-3-3 binding to LRRK2 is disrupted by multiple Parkinson's disease-associated mutations and regulates cytoplasmic localization. *Biochem J*. 2010;430(3):393-404. doi:10.1042/BJ20100483
13. Usmani A, Shavarebi F, Hiniker A. The Cell Biology of LRRK2 in Parkinson's Disease. *Mol Cell Biol*. 2021;41(5):e00660-20. Published 2021 Apr 22. doi:10.1128/MCB.00660-20
14. Miklossy J, Arai T, Guo JP, et al. LRRK2 expression in normal and pathologic human brain and in human cell lines. *J Neuropathol Exp Neurol*. 2006;65(10):953-963. doi:10.1097/01.jnen.0000235121.98052.54
15. Marchand A, Drouyer M, Sarchione A, Chartier-Harlin MC, Taymans JM. LRRK2 Phosphorylation, More Than an Epiphenomenon. *Front Neurosci*. 2020;14:527. Published 2020 Jun 16. doi:10.3389/fnins.2020.00527
16. Drouyer M, Bolliger MF, Lobbestael E, et al. Protein phosphatase 2A holoenzymes regulate leucine-rich repeat kinase 2 phosphorylation and accumulation. *Neurobiol Dis*. 2021;157:105426. doi:10.1016/j.nbd.2021.105426
17. Taymans JM, Fell M, Greenamyre T, et al. Perspective on the current state of the LRRK2 field. *NPJ Parkinsons Dis*. 2023a;9(1):104. Published 2023 Jul 1. doi:10.1038/s41531-023-00544-7

18. Goveas L, Mutez E, Chartier-Harlin MC, Taymans JM. Mind the Gap: LRRK2 Phenotypes in the Clinic vs. in Patient Cells. *Cells*. 2021;10(5):981. Published 2021 Apr 22. doi:10.3390/cells10050981
19. Tasegian A, Singh F, Ganley IG, Reith AD, Alessi DR. Impact of Type II LRRK2 inhibitors on signaling and mitophagy. *Biochem J*. 2021;478(19):3555-3573. doi:10.1042/BCJ20210375
20. Wojewska DN, Kortholt A. LRRK2 Targeting Strategies as Potential Treatment of Parkinson's Disease. *Biomolecules*. 2021;11(8):1101. Published 2021 Jul 26. doi:10.3390/biom11081101
21. Baptista MAS, Merchant K, Barrett T, et al. LRRK2 inhibitors induce reversible changes in nonhuman primate lungs without measurable pulmonary deficits. *Sci Transl Med*. 2020;12(540):eaav0820. doi:10.1126/scitranslmed.aav0820
22. Reynolds A, Doggett EA, Riddle SM, Lebakken CS, Nichols RJ. LRRK2 kinase activity and biology are not uniformly predicted by its autophosphorylation and cellular phosphorylation site status. *Front Mol Neurosci*. 2014;7:54. Published 2014 Jun 24. doi:10.3389/fnmol.2014.00054
23. Marchand A, Sarchione A, Athanasopoulos PS, et al. A Phosphosite Mutant Approach on LRRK2 Links Phosphorylation and Dephosphorylation to Protective and Deleterious Markers, Respectively. *Cells*. 2022;11(6):1018. Published 2022 Mar 17. doi:10.3390/cells11061018
24. Morrison DK. The 14-3-3 proteins: integrators of diverse signaling cues that impact cell fate and cancer development. *Trends Cell Biol*. 2009;19(1):16-23. doi:10.1016/j.tcb.2008.10.003
25. Obsilova V, Obsil T. Structural insights into the functional roles of 14-3-3 proteins. *Front Mol Biosci*. 2022;9:1016071. Published 2022 Sep 16. doi:10.3389/fmolb.2022.1016071
26. Paul AL, Denison FC, Schultz ER, Zupanska AK, Ferl RJ. 14-3-3 phosphoprotein interaction networks - does isoform diversity present functional interaction specification?. *Front Plant Sci*. 2012;3:190. Published 2012 Aug 20. doi:10.3389/fpls.2012.00190
27. Ballone A, Centorrino F, Ottmann C. 14-3-3: A Case Study in PPI Modulation. *Molecules*. 2018;23(6):1386. Published 2018 Jun 8. doi:10.3390/molecules23061386
28. Pennington KL, Chan TY, Torres MP, Andersen JL. The dynamic and stress-adaptive signaling hub of 14-3-3: emerging mechanisms of regulation and context-dependent protein-protein interactions. *Oncogene*. 2018;37(42):5587-5604. doi:10.1038/s41388-018-0348-3
29. Kaplan A, Ottmann C, Fournier AE. 14-3-3 adaptor protein-protein interactions as therapeutic targets for CNS diseases. *Pharmacol Res*. 2017;125(Pt B):114-121. doi:10.1016/j.phrs.2017.09.007
30. Stevers LM, Sijbesma E, Botta M, et al. Modulators of 14-3-3 Protein-Protein Interactions. *J Med Chem*. 2018;61(9):3755-3778. doi:10.1021/acs.jmedchem.7b00574
31. Shen YH, Godlewski J, Bronisz A, et al. Significance of 14-3-3 self-dimerization for phosphorylation-dependent target binding. *Mol Biol Cell*. 2003;14(11):4721-4733. doi:10.1091/mbc.e02-12-0821
32. Cao W, Yang X, Zhou J, et al. Targeting 14-3-3 protein, difopein induces apoptosis of human glioma cells and suppresses tumor growth in mice. *Apoptosis*. 2010;15(2):230-241. doi:10.1007/s10495-009-0437-4

33. Wu H, Yao H, He C, et al. Molecular glues modulate protein functions by inducing protein aggregation: A promising therapeutic strategy of small molecules for disease treatment. *Acta Pharm Sin B*. 2022;12(9):3548-3566. doi:10.1016/j.apsb.2022.03.019
34. Giusto E, Yacoubian TA, Greggio E, Civiero L. Pathways to Parkinson's disease: a spotlight on 14-3-3 proteins. *NPJ Parkinsons Dis*. 2021;7(1):85. Published 2021 Sep 21. doi:10.1038/s41531-021-00230-6
35. Somsen BA, Ottmann C. Challenges of studying 14-3-3 protein-protein interactions with full-length protein partners. Biophys J. 2022 Apr 5;121(7):1115-1116. doi: 10.1016/j.bpj.2022.03.007. Epub 2022 Mar 9. PMID: 35320703; PMCID: PMC9034296.
36. Lavalley NJ, Slone SR, Ding H, West AB, Yacoubian TA. 14-3-3 Proteins regulate mutant LRRK2 kinase activity and neurite shortening. *Hum Mol Genet*. 2016;25(1):109-122. doi:10.1093/hmg/ddv453
37. Sears RM, May DG, Roux KJ. BioID as a Tool for Protein-Proximity Labeling in Living Cells. *Methods Mol Biol*. 2019;2012:299-313. doi:10.1007/978-1-4939-9546-2_15
38. Deniston CK, Salogiannis J, Mathea S, et al. Structure of LRRK2 in Parkinson's disease and model for microtubule interaction. *Nature*. 2020;588(7837):344-349. doi:10.1038/s41586-020-2673-2
39. Fraser KB, Moehle MS, Daher JP, et al. LRRK2 secretion in exosomes is regulated by 14-3-3. *Hum Mol Genet*. 2013;22(24):4988-5000. doi:10.1093/hmg/ddt346
40. Taymans JM, Mutez E, Sibran W, et al. b Alterations in the LRRK2-Rab pathway in urinary extracellular vesicles as Parkinson's disease and pharmacodynamic biomarkers. *NPJ Parkinsons Dis*. 2023b;9(1):21. Published 2023 Feb 7. doi:10.1038/s41531-023-00445-9